1-1-1979

An investigation of the modification of pore morphology during the densification of pressure-sintered CoO.

Andrew D. Miro

AN INVESTIGATION OF THE MODIFICATION OF PORE MORPHOLOGY DURING THE DENSIFICATION OF PRESSURE-SINTERED CoO

by

Andrew D. Miro

A Thesis
Presented to the Graduate Committee
of Lehigh University
in Candidacy for the Degree of
Master of Science
in
Metallurgy and Materials Engineering

Lehigh University
1979

CERTIFICATE OF APPROVAL

This thesis is accepted and approved in partial fulfillment of the requirements for the degree of Master of Science.

August 12, 1979
(date)

Professor in Charge

Chairman of Department

ACKNOWLEDGEMENTS

It is very difficult to single out any one person to express my gratitude for being associated with the Department of Metallurgy and Materials Engineering, and for all the courtesies they extended to me in my two years at Lehigh. However, the following people must be mentioned for the assistance and patience they afforded me here at Lehigh.

First of all, I would like to thank Gene Kozma, Paul Urick, and Doug Bush for all the technical assistance they gave me, and Louise and Betty for their typing skills.

Secondly, I would like to thank every member of the "ZOO" for their warm greetings in the morning, their enlightening discussions, and their ever-present sense of humor.

Thirdly, I want to express my gratitude to Dilip Subramanyam and Steve Baumann for helping me in my studies, their moral support, and especially their friendship.

Finally, my deepest thanks go to Barry Bender and Dr. Notis. I want to thank Barry for his patience, good sense of humor, and for putting up with me for two years. My thanks to Dr. Notis are infinite because without his guidance, patience, knowledge, and good sense of humor, I never would have made it. I would also like to thank Dr. Notis' family for making me feel at home during the holidays.

TABLE OF CONTENTS

LIST OF TABLES

LIST OF FIGURES

ABSTRACT

An automatic system for quantitative image analysis was developed to study the transition from intermediate to final stage pore structure in pressure-sintered CoO. In addition, macroscopic density measurements were utilized to study this variation.

Macroscopic density measurements indicate a linear decrease in open porosity from approximately 24% total porosity to approximately 9% total porosity. Concurrently, the amount of closed porosity is initially a constant fraction of about 6% but finally decreases to zero as the density increases.

One of the significant results from quantitative image analysis shows that the average projected length of pores appears to be a good parameter to quantitatively describe the transition from closed to cylindrical open porosity. Quantitative image analysis indicates that a linear relation between the ratio of mean pore radius and mean grain size (r/G) versus total porosity (P) is observed throughout the entire density range studied. This result appears to be a significant experimental verification of the Zener relation and its applicability to sintered systems.

I. INTRODUCTION

Hot-pressing is an important method of ceramic processing that permits the formation of higher density products at lower temperatures and/or in shorter times than conventional pressureless sintering. Hot-pressing and pressureless sintering are thought to be very similar because it is believed that for both of these methods, the same atomistic mechanisms contribute to densification. Therefore, the microstructure should develop in a similar if not identical way as the density increases. However, the major advantage of hot-pressing over pressureless sintering is the order of magnitude increase in driving force for densification due to the applied pressure without a concurrent increase in the driving force for grain growth.

During the hot pressing process[1] the pore-grain structure passes through three individual configurations or stages. The initial stage includes the formation of bonds and growth of necks at the particle contact points which occur upon heating the powder to an elevated temperature and upon application of the stress. When the interparticle necks have grown to a substantial size relative to the particle diameter and the surfaces have begun to smooth out, the pore-grain geometry enters the intermediate stage. The porosity during the intermediate stage (to approximately 85% of theoretical density) is commonly in the form of a continuous network of cylindrical pores which

are centered along the grain edges and interconnected at grain corners. As the relative density of the material increases under these conditions, some pores become isolated from the continuous network. This isolation of pores continues until effectively all the pores are isolated within the material and are generally located at grain corners. This condition of completely closed porosity comprises the final stage which occurs at approximately 95% TD. Therefore, between 85% and 95% TD, which may be termed the transition stage, there exists both interconnected (or open) and closed porosity.

The variation in open and closed porosity as a function of porosity has been investigated on the macroscopic level by Arthur[2] on copper powder. Arthur showed that there is a smooth linear decrease in open porosity from ≈60% density to ≈95% density. This was accompanied by a constant small fraction of closed porosity until about 85% density. At this point, the amount of closed porosity increased and the amount of open porosity decreased until only closed porosity remained at ≈95% density. At this point the closed porosity equals the total porosity and there is a slow decrease in closed porosity until full density is achieved.

This variation in open and closed porosity has also been observed in ceramic materials. Coleman and Beere[3] in their work on UO_2 showed that when the volume fraction of open porosity decreases to 0.15, closed porosity began to form. When the

volume fraction of porosity reached 0.05, only closed porosity was present. Budworth[4] also showed that the pore network remain entirely open until about 85% TD. At that point closed porosity begins to be detectable. Therefore, general intermediate stage behavior is expected from its beginning up to ≈85%. Up to this density all existing porosity should exist as a continuous network of cylindrical pores.

It will be the purpose of this investigation to study this modification of pore morphology using density measurements and quantitative image analysis. In addition, the concurrent process of grain growth will be examined. Therefore, with an understanding of these two processes as a function of density, we will be able to modify existing hot-pressing models and examine the consequences of complex microstructure to densification behavior.

II. BACKGROUND

A. Past Studies on the Intermediate Stage of Sintering

Despite the complex nature of porosity during the intermediate stage of sintering, simplified models of the pore morphology have been presented in the past.[5,6,7] This simplification of the pore morphology has enabled quantitative calculation of the densification rate. One of the best known models is that of Coble.[5,6] In Coble's model, it was assumed that one densification mechanism operates, either volume diffusion or grain boundary diffusion. Furthermore, a specific geometry was assumed. Coble[5] fitted cylinders around the edges of a tetrakaidecahedron shaped grain. The tetrakaidecahedron has the property of fitting together without leaving gaps between the faces and the porosity arises solely from the continuous network of cylinders. Due to this well defined geometry, the shrinkage of the compact is reduced (assumed to occur by uniform shrinkage of these pores) but without a change in grain size or shape.

Coble's model has been refined in recent years by Eadie and Weatherly[8] and Beere.[7] Eadie and Weatherly used the same geometrical model as Coble[5,6] but the sintering rate of cylindrical porosity was calculated more thoroughly. Beere[7] used a tetrakaidecahedron geometry but replaced the cylinders by complex shapes which have constant surface curvature and satisfy

the balance of tensions at the pore boundary intersections. Kuczynski[9] has criticized these simplified geometrical models[5,8] because they do not take into account the Ostwald ripening of the pores which is an essential part of the densification process. In a system of non-uniform pores and grains, pore shrinkage and simultaneous increase of their average size occur, as well as that of the crystalline grains. These two processes are mutually interdependent. In Coble's[5,6] model, as well as Eadie and Weatherly, and Beere, these processes are not incorporated.

Another model[10] for the intermediate stage of sintering has been proposed which is somewhat similar to Coble's model but tries to overcome the problem of grain growth during densification. Johnson[9] proposed a model which relates the densification rate to the instantaneous geometry in the compact and to the volume and grain boundary diffusion coefficients. The model assumes that pore and grain growth may occur simultaneously during densification. The geometrical parameters are measured using basic quantitative stereological methods. With these geometrical parameters, a description of the evolution of the microstructure and calculated values for the grain boundary and/or volume diffusion coefficients can be obtained using the following equation[6]

$$\frac{x}{\bar{H}L_v}\,\frac{dV}{dt} = \frac{8\,\gamma\,\Omega\,D_v}{kT}\,\frac{S_v}{L_v} + \frac{8\,\gamma\,r\,b\,D_s}{kT} \qquad (1)$$

where x = average diffusion distance, assumed to be 1/4 the average grain diameter, L_v = grain boundary-pore intersection length/unit volume, S_v = pore surface/unit volume, $\bar{H}$ = mean pore surface curvature, (1/V) (dV/dt) = rate of fractional volume shrinkage, V = volume of compact, γ = surface tension, Ω = volume transported/ion of slower moving species, D_V = volume-diffusion coefficient, D_b = grain boundary diffusion coefficient, b = grain boundary width, and kT has its usual meaning.[7] By plotting the left side of Equation 1 vs. (Sv/Lv), Dv and bD_g are obtained from the slope and intercept respectively.

More recently, other models have been proposed which incorporate the effects of grain growth. Rosolowski and Greskovich[11] have developed a semiempirical model for intermediate stage sintering based on simultaneously occuring volume and grain boundary diffusion mechanisms of mass transport and they explicitly incorporate the effects of grain growth. In this model, it was assumed that pores were cylindrical and located on grain edges but they allowed a distribution of radii to occur, and not all edges had to contain pores. Their sintering equation depends strongly on the reduction of pore number density associated with grain growth and is independent of the mechanism of grain growth.

In the development of Rosolowski and Greskovich's[11] intermediate stages sintering equation, an underlying assumption was made that the average grain size was proportional to average pore size. This assumption was based on comparison to the final

stage of sintering. During the final stages of sintering, when there are isolated pores at grain corners, the average pore size has been observed to increase because of coalescence resulting from grain growth. This process occurred in a manner such that the ratio of the average grain size to pore size remained approximately constant. Therefore, these authors[11] assume that a similar effect occurs during the intermediate stage and incorporated this ratio as a constant. However, Rosolowski and Greskovich provide no experimental evidence for these assumptions.

In the literature, experimental evidence has been given for the relation between grain size and density[12,13,14] during intermediate stage sintering, but information is sparce on the relation between pore size and grain size.[27] Recent analysis by Gupta[12] and Samanta and Coble[13] have shown that in several cases, grain size is linearly related to the density during the intermediate stage of sintering, irrespective of the sintering temperature. Francois and Kingery,[27] to a limited extent, have monitored grain growth and pore growth as a function of time and temperature in UO_2 for two different pore morphologies. In samples with essentially intragranular porosity, measured values of the ratio of mean pore diameter/mean grain diameter were taken of pores situated at grain boundaries. This ratio decreases with time at temperature while at the same time the density is increasing. Different behavior is found for samples

with intergranular porosity. The same measurements were taken and the ratio of mean pore diameter/mean grain diameter remained essentially constant with time at temperature. However, the amount of data obtained by Francois and Kingery[27] is small and any trends observed are inconclusive. It appears, however, that grain and pore growth are important processes and must be incorporated into intermediate stage sintering models.

Kuczynski[9] has recently considered the problem of Ostwald ripening in powder compacts on a statistical basis. He assumes that, at constant porosity, the average pore size is related to the average grain size, an assumption consistent with the Zener relation, $\bar{r}/\bar{G} = K P$, where $\bar{r}$ = mean pore radius, $\bar{G}$ = mean grain size, P = porosity, and K = constant. In Kuczynski's statistical approach, the intermediate stage of sintering is modelled by a continuous cylindrical pore of variable diameter meandering through a solid, crossing itself and with time develops dead end branches. Therefore, this model has no assumed grain geometry and takes into account the effects of pore and grain growth as a function of porosity.

Wingert and Notis[16] have proposed a model based on Coble's model, but have incorporated the effects of pore and grain growth, and the variation of open and closed porosity. The effects of pore and grain growth are incorporated into the model by the factor Z_I. This factor, which is less than or equal to 1 represents the fraction of grain boundaries which are occupied

by a cylindrical pore at a given time during the intermediate stage. The factor Z_I will correct the original assumption made by Coble[5] that each grain edge is occupied by a cylindrical pore. From the following discussions it will be apparent that only a fraction of the grain edges are actually occupied by porosity.

The expression for Z_I was derived from the following expression for the relative bulk porosity:

$$P = 25.83 \left(\frac{r}{G}\right)^2 (Z_I)$$

It is assumed that at the inception of the intermediate stage ($P = P_o$, $P_o = .25$) each grain edge is occupied by a cylindrical pore (i.e. $Z = 1$ at $P = P_o$) so from the above equation, $P_o = 25.83 \left(\frac{r}{G}\right)^2$. Assuming that r remains proportional to G throughout the intermediate stage, the proportionally constant $Y = \frac{r}{G}$ is given by $Y = (P_o/25.83)^{\frac{1}{2}}$. Knowing Y, the fraction of grain edges occupied by cylindrical pores can now be calculated at any time during the intermediate stage as:

$$Z_I = 0.387 \frac{P}{Y2}$$

Therefore, the effect of r/G is incorporated into the model. Our experimental results will be substituted into the model to test its validity.

Wingert and Notis[16] have also incorporated the variation of open and closed porosity during the transition stage in the following way. At any point during the transition stage a certain

fraction of the porosity will exist as a continuous network of cylindrical pores characteristic of the intermediate stage, while the rest has become isolated in a configuration as exists during the final stage. Therefore, the fraction of material having an intermediate type pore structure, alpha, is expected to densify locally according to the intermediate stage model while simultaneously the remaining fraction of material, beta, has a final stage type pore configuration and densifies locally according to the final stage model.

According to the model[18] at the .85 relative density or below, alpha = 1.0 and beta = 0, and at .95 relative density, alpha = 0 and beta = 1. This is a result of the assumption that the cylindrical pores pinch off and isolate pore pockets steadily until all the porosity is isolated at .95% relative density. Therefore, in the simplest model possible, alpha is assumed to decrease and beta is assumed to increase linearly with relative density during the transition stage (see Fig. 1).

B. Quantitative Image Analysis

The quantitative description of microstructural development is a complex problem. Direct observations and manual measurements are generally impractical due to the time and effort required to disassemble the body and measure all the appropriate parameters to describe its structure. Instead, stereological and statistical methods can be applied to deduce the structure

of the total bulk solid from a limited number of surfaces. The accuracy depends on how representative the surfaces we examine and how representative the limited number of observations are of the entire structure. Other factors which affect the accuracy are the specimen preparation and the type and accuracy of the measurement made. All of these factors need to be considered when establishing procedures for examination of a specimen.

Until recently, the quantitative description of microstructure required laborious manual measurements of the features of interest. However, the development of semi- and full-automated instruments for quantitative image analysis has provided fast, precise, and reliable ways to obtain these measurements. One such instrument is a Millipore πMC Particle Measurement Computer. The Millipore[17] provides three basic types of information: 1) counts - number of particles (field or chosen area); 2) measurements - details of particle parameter including summation or averaging (projected area, projected length, Feret's diameter, maximum chord (see Fig. 2)); and 3) size distributions. The basic operating principles and function of the Millipore πMC are as follows:[17]

When a specimen is placed in a microscope (optical microscope, SEM, or TEM) its image is detected and is passed to a television monitor. The signal also passes to a circuit in which all particles, selected particles, or selected field areas are

detected. The signals are then processed through the basic computer module and other computational elements chosen according to the parameters required. The results of counts or measurements are shown along the top of the field image on the television monitor. Since all calculations are carried out within the computer, all results are shown directly in micrometers or square micrometers. A schematic of this operation is shown in Figure 8.

In counting and measuring automatically, the πMC is capable of defining accurately the boundaries of a particle regardless of particle shape. The πMC method of detection is as follows (Figure 3). When a sweep encounters the boundary of a particle, the difference in light intensity of the particle from its background is sensed by the threshold circuitry. The trailing edge of the particle is similarly sensed (x,y). On the following sweep (y + 1) the instrument begins to scan for the particle boundary in advance (X - Δ) of the position detected on the previous sweep. If the leading edge of the particle has not been detected before this point of time, the instruments logic indicates that the entire boundary has been sensed and measurement is terminated. The logic used in this method of detection avoids re-entrant errors and prevents recording of more than a single particle.

Particles may vary widely in hue against a background. A

black particle on a white background, or vice versa, is easy to detect but a transparent particle presents a more difficult problem. The effects of different types of images is referred to as Grey Scale Values. The Millipore πMC uses three threshold modes of detection to overcome this problem of verifying images (see Fig. 4).

In the manual mode of operation, only those particles producting a video signal pulse above an arbitrarily chosen D.C. voltage level are detected. This allows the operator to manually select this detection level and select the particles being counted or measured. Using the semi-automatic setting, detection is determined by the video signal difference between the particle and the background in the vicinity of the particle but peaking occurs at the 50% level to give high reproducibility in particle measurement. The semi-automatic control is variable giving the operator the ability to provide selective measurement of particles varying in Grey Scale Value. The fully automatic mode of detection is the most sensitive and allows virtually all particles resolvable by the video system to be detected regardless of their greyness. In both automatic and semiautomatic modes of operation, threshold triggering occurs at the mid-point of the particle intensity profile providing precise measurements. One important point to note is that the operator can rapidly check which particles are being detected. In counting, the particles are "tagged" (Fig. 5a), in measuring (Fig. 5b) the

particles are outlined.

The information obtained from the πMC is based on four parameters which are maximum horizontal chord, Feret's diameter, projected length, and projected area. The first three measurements are orientation dependent but projected area is independent of particle orientation.

In addition to the modules for counting and size measurement, there are also plug-in components used in conjunction with the size measurement module to provide both oversize counts based on selected horizontal chords, and individual particle examination with a selective light pen (Fig. 6). Selection of oversize chords is made simply by adjustment of a controlling dual potentiometer. By using the oversize count facility, a distribution based on large numbers of particles can be obtained easily and speedily. The ability to handle large numbers of particles provides a statistically valid result and minimizes any error due to particle orientation.

The measurements performed by the Millipore πMC will provide valuable information in characterizing the microstructural development in this present study. By obtaining a pore size distribution, a mean pore size, a mean grain size, and a mean projected length of a specific site, we will be able to characterize that site. If this procedure is done to a number of sites at various density levels, we will be able to relate these values

to the stage of microstructural development that characterizes the material.

III. EXPERIMENTAL PROCEDURE

A. Material Selection

Cobalt monoxide was chosen as the material system in which to study the variation in pore morphology during the transition from intermediate to final stage pore structure. It was selected because it is a well studied material in areas pertinent to the present work because it is single phase, exhibits little or no discontinuous grain growth, and because of the availability of high purity powders. In the literature, there is documented diffusion data,[18] along with creep studies,[19] sintering, and hot-pressing work.[20] Previous studies have also shown that during hot-pressing[20] the pores remain attached to the grain boundaries and are most commonly located at the grain corners at high densities.

B. Powder Preparation

Two different batches of fine grained high purity Co_3O_4 (Johnson Matthey Puratronic, Batch 1, S.85993, Batch 2, S.7023) were used as the starting powders. The conversion to CoO, which is the stable phase at 2.2×10^{-2} MPa O_2 and at >1193 Å was achieved by heating the powder at 1223 °K for 28800 sec. in high purity Al_2O_3 crucibles and then air quenching to prevent the reformation of Co_3O_4. X-ray diffraction indicated that complete conversion to CoO was not always achieved; complete conversion

to CoO was accomplished by a short thermal treatment in the vacuum hot press as described in the next section. The air-fired and quenched powders were ground with mortar and pestle and passed through a 325 mesh sieve prior to use.

C. Vacuum Pressure - Sintering

Pressure sintering was performed in a vacuum hot-pressing furnace in which pressure was applied axially through two vertical rams; the lower ram is rigidly mounted to the frame, and the upper ram is connected to a hydraulic actuator mounted on the top of a frame. The ambient vacuum level was controlled with a fine metering valve which was used to bleed atmosphere into the chamber.

The die assembly (Fig. 7) included two plungers 2.54 cm in diameter and a die 3.81 cm ID and 7.62 cm OD, all made of an Mo-0.5% Ti-0.08% Zr wrought alloy (TZM, Climax Molybdenum Company). High purity Al_2O_3 spacers and sleeves separated the sample from the alloy to prevent reaction. To facilitate removal of the specimen from the spacers and sleeves, they were slurry-coated with a thin layer of BN. The die wall contained two cylindrical cavities into which Pt-Pt 10 Rh thermocouples were inserted to monitor the temperature.

Approximately 20 grams of loose powder were loaded into the die assembly. The chamber was sealed and pumped down to 10 μm with a mechanical pump. The temperature was raised to

773 ± 50°K and held for 3600 sec. to degas the sample. The temperature was then raised to 1273 ± 50°K and held for 5400 sec. in order to achieve complete conversion to CoO. This was later verified by examination of specimens in an SEM equipped with an energy dispersive spectrometer; the presence or absence of the Co_3O_4 second phase could easily be verified by comparing CoK_α peak intensities to that from the matrix phase.

The applied pressure was then raised to the desired level and the temperature was maintained or quickly increased to that of interest (± 10°K). At the same time the vacuum level inside the chamber was adjusted to 50 μm by using an air-inlet metering valve. Densification was monitored by the movement of the upper ram on which both a dial micrometer and the core of a linear variable differential transformer were mounted. The signal from the LVDT was fed to an X-Y recorder which plotted ram movement as a function of time. The dial micrometer was read periodically as a check on the recorder plot. The ram movement thus recorded is equal to the change in height of the specimen minus the thermal expansion of the plunger and rams. Therefore, thermal expansion curves were obtained for each temperature of interest; these results were added to the X-Y plots of ram movement to derive the actual change in sample height with time.[20] The specimens were pressure-sintered to pre-determined density levels; at this point the applied load was removed and the specimens were slowly cooled (at

.06°K/sec.) to room temperature.

D. Porosity Measurements Using Archimedes Liquid Displacement Technique

The specimens were immersed in a small beaker filled with toluene and were then placed in a vacuum dessicater in which the pressure was reduced for approximately 1800 sec. This treatment removed gas from the open pores by replacement with toluene. The specimens were weighed while immersed in toluene and were then removed from the toluene and, immediately after the surface had been wiped with weighing paper, then weighed in air. Letting W_D = dry weight of specimen; W_I = weight of specimen in toluene; W_S = weight of impregnated specimen in air; P_X = theoretical X-ray density of CoO; and ρ_T = density of toluene then:

$$\% \text{ TOTAL POROSITY } (P_T) = 1 - \frac{W_D \rho_T}{(W_S - W_I)\rho_X} \quad 100$$

$$\% \text{ OPEN POROSITY } (P_O) = \frac{W_S - W_D}{W_S - W_I} \quad 100$$

$$\% \text{ CLOSED POROSITY } (P_C) = P_T - P_O$$

A method employed by Arthur[2] was also used on a number of specimens; in this latter method, the specimen is also weighed

in water after impregnation with toluene. However, since Arthur's method gave identical results to the preceding method, it was not routinely used because of the simplicity of the toluene displacement method.

E. Quantitative Image Analysis

1. Specimen Preparation. The specimens were prepared for metallographic measurements by first impregnating with a lead borosilicate frit (Ferro Frit No. 3419) pre-saturated with CoO. Lead borosilicate frit is a good impregnating agent because it is fluid at a fairly low temperature ($\approx$810°K) and penetrates well into fine surface connected pores. Another advantage of this frit system is that its Youngs modulus is $\approx 70 \times 10^3$ MPa[21] compared to that of 227.3×10^3 MPa[22] for CoO; this high modulus provides high strength and good interfacial matching with CoO.

The specimens were then polished using a series of 3 μm, 1 μm and .25 μm diamond plates for the final polish. The specimens were etched[15] at room temperature using a mixture of lactic (90%), nitric (7.5%), and hydrofluoric acides (2.5%).

2. Microstructural analysis. Quantitative measurement of the microstructural development in CoO was performed on the polished sections using an ETEC SEM which was interfaced with a Millipore πMC Particle Measurement Computer (see schematic Fig. 8). The interfacing unit is a Vistascan (ETEC Corporation)

video information storage and processing system. The interfacing unit[23] permits signal storage, integration display, and subsequent replay for recording. The stored image may be visually displayed or recorded directly from the SEM CRT at the fastest speed scan compatible with line resolution. Further the stored image is not materially degraded by being recorded, and therefore can be used more than once. The system also operates with a Wang 600 in-line computer which allows direct computation of various statistical parameters, and particle size distribution.

Since the Millipore πMC is basically a grey level detector, the advantage of this combined system lies in its ability to alter the grey levels while storing the image. This allows maximization of the difference in grey levels between the pores and the matrix.for optimum detection by the Millipore πMC.

The πMC particle measurement computer is capable of measuring features at a minimum detection level of 1/200th of the field of view. Therefore, magnifications of 800X-4000X were used in order to measure the pore sizes which ranged from .345 μm to 1.20 μm.

Random selection of sites was employed with two restrictions; locations with large features that obscured observation of the smaller ones were avoided as were areas with atypical porosity internal to the grains. For the results given below approximately

40 sites (data sets) were examined, each of which contained as few as 150 pores or as many as 650 pores, depending on the sample. The number of pores observed depended on the porosity level and the magnification used. By examination of many sites with 150-650 features in each site, it was felt that a statistically reliable set of data was obtained.

The grain size was measured using a linear intercept technique developed by Mendelson.[24] However, when the amount of porosity exceeds 5-10 vol% corrections to this method have to be applied to achieve an accurate measurement. Therefore, a method developed by Wurst and Nelson[25] was used which corrected Mendelson's method for the effect of porosity in the structure.

The πMC Millipore was calibrated to the ETEC SEM through the use of a copper grid of known dimensions. Calibration factors appear in Table I.

IV. EXPERIMENTAL RESULTS AND DISCUSSION

A. Powder Characterization and Pressure Sintering

Prior to hot-pressing, the two batches of CoO were examined with the SEM. Batch 1 (Fig. 9a) appears to be fine grained, unagglomerated, dense, and pore-free while Batch 2 (Fig. 9b) has a much larger particle size but with a very porous appearance. The resulting microstructures obtained after hot-pressing (Fig. 4a, b) are very different. The dense pore-free powder produces a microstructure (Fig. 10a) with pores generally located at the grain boundaries, while the porous powder produces a microstructure (Fig. 10b) with pores internal to the grains. Since the microstructure development related to porosity at the grain boundaries is the area of immediate interest for this investigation, further results pertain to those samples fabricated from the Batch No. 1 powder. Any porosity internal to the grain would prove to be experimentally difficult to handle, and therefore, specimens fabricated from the porous powder were eliminated from further study.

A series of specimens were hot-pressed with densities ranging from the intermediate to final stage of sintering using the dense pore-free powder. Table II lists the hot-pressing conditions and final densities for each of the specimens; the temperature and times were varied in order to achieve the various

desired porosity levels. The resulting porosity levels varied from 3.78% to 24.25%.

Density gradients that existed within each sample allowed the measurement of different porosity levels in different areas of the same sample, thus eliminating the need to hot-press specimens at each porosity level. For example, a series of SEM micrographs (Fig. 11), all taken from the same low density sample, show areas ranging from 17% to 12% porosity. SEM micrographs obtained on a higher density sample are shown in Figure 12. In the first micrograph (Fig. 12a) the majority of the pores are located at the grain corners, but some cylindrical porosity still remains; πMC measurements indicate this area to have 6% total porosity. Most of the pores appear to be in the process of pinching off and therefore this area appears to be representative of a situation just entering the final stage of sintering. The next micrograph (Fig. 12b) is a site on the same specimen which is well into the final stage; all the pores in the micrograph are closed and at the grain boundaries. Figure 13 is a higher magnification shot of the previous micrograph showing a typical microstructure of a high density specimen of CoO.

B. Macroscopic Porosity Measurements

The variation in open and closed porosity as a function of

total porosity measured by the liquid displacement technique is shown in Figure 14. There appears to be a linear decrease in open porosity from approximately 24% total porosity to approximately 9% total porosity. Duplicate samples measured with Hg porosimetry indicate almost identical results (see Appendix I). There are no data points at lower porosity levels but it is assumed from the literature[2, 3, 15] that open porosity approaches zero at approximately 5% total porosity. The amount of closed porosity is initially a constant fraction of about 6% but finally decreases to zero as the density increases. The curve for open porosity is almost identical to that obtained during sintering of copper by Arthur.[2] However, Arthur's results for closed porosity indicate only a small fraction of closed porosity (<1%) from approximately 40%-15% total porosity. Arthur reported the amount of closed pores to increase to a maximum at 5% porosity and then slowly decrease until full density was achieved. Similar results have recently been observed during sintering of ZnO.[28] The abnormally high level of closed porosity obtained by macroscopic measurements in our samples may be explained by examination of the microstructure shown in Figure 15. There is a small amount of porosity with large radius that is internal to the grains and which would significantly contribute to the level of closed porosity. Another contribution to the high apparent closed porosity level would be the density

gradients present in the specimens (Figs. 11 and 12) i.e., a higher density and structure typical of the final stage near the specimen surface would tend to indicate an erroneously high closed porosity level near the lower density center of the specimen. Even though the specimens had some porosity internal to the grains, this porosity was very localized; at the microstructural level used for quantitative metallography we were able to examine areas of the specimen with porosity typically located on the grain boundaries.

C. Quantitative Image Analysis

In order to characterize the porosity on each site examined with the SEM, the following measurements were obtained with the Millipore πMC: average fractional pore area (both grain boundary and internal porosity), pore size distribution, mean pore size, and the mean projected length of the pores. In addition, a micrograph was taken for each site examined and the grain size calculated from the micrographs.

The average fractional pore area was measured for each site examined by taking the total area of the pores and dividing it by the total area of the site. An average value of the porosity measured by the Millipore πMC was then calculated and compared to immersion density measurements (Table II). Some of the samples show a significant difference between the two measurements. This

is attributable to the sampling of specific sites by the operator; certain porosity levels were desired for evaluation at various times during the investigation, others were not. Therefore, the sample was not scanned from end to end to get a good average value for the porosity.

The area of the pores that are internal to the grains was measured using the light pen on each site examined that contained internal porosity. Figure 16 is a plot describing the amount of internal porosity on each site. In this graph there are two curves, total porosity and grain boundary porosity. The curve of the total porosity is drawn on this graph to show that if all the porosity is located on the grain boundaries, then this is the curve that represents this situation. The other curve is the actual amount of grain boundary porosity measured with the Millipore πMC. Therefore, the difference between these two curves is the amount of porosity internal to the grains. The amount of internal porosity is then generally less than 0.5% of the total porosity on the sites chosen for our analysis. Therefore, we were able to examine sites that had little or no internal porosity, even though the specimens might contain a higher degree of internal porosity as described earlier.

The next step was to obtain a pore size distribution. This was obtained through the use of the oversize count function on the Millipore πMC. The oversize count function counts all pores

in a field having a maximum horizontal chord greater than a selected lower size limit. Since this is a measure of N_A (pore number per unit area), which is a two-dimensional quantity, Saltikov's[26] method (see Appendix I) is employed to obtain N_V, which is the three-dimensional equivalent. Therefore, a distribution plot of N_V vs. pore diameter was obtained from each site examined.

From each of these distributions a mean pore radius was obtained. In addition, the mean grain size was obtained from the sites from which the pore size distribution were calculated. Therefore, a mean pore radius and a mean grain size were obtained for a series of porosity levels ranging from the intermediate stage to the final stage. These values are listed in Table IV. The ratio of the pore radius to grain size (r/G) is plotted as a function of total porosity in Figure 17. The plot of r/G vs. P gives a linear relationship which is consistent with a Zener relationship. The Zener relationship states that $r/G \sim P$, and will be discussed below. The significance of this finding to sintering theories and its incorporation into the Wingert model will also be dealt with later in this paper.

Figure 18 is a plot of N_V vs. pore diameter for the final stage of sintering. Although there is no definite trend to the data, the general trend is that as the porosity increases the size and number of pores increase. However, in order to quantitatively describe the change in the pore size distribution

as a function of porosity, a more complete study is needed.

In order to obtain a qualitative picture of the change in the number of pores vs. pore diameter as a function of porosity Figure 19 was generated. Figure 19 is a plot of log percent pores greater than vs. pore diameter at various porosity levels ranging from the intermediate to final stage of sintering. This plot was obtained by converting the values of N_V to percent pores greater than and taking the log of this value. This graph shows that as porosity is increased the number and size of pores will increase. This result is again consistent with the observation that the number density of pores reduces as density is increased.

Another measurement that was generated by the Millipore ΠMC was the mean projected length of the pores. Figure 20 shows a plot of mean projected length vs. total porosity. This graph shows that as the total porosity increases the projected length will increase until a certain porosity level, at which point the projected length tends to become a constant value. In terms of relating the projected length to the change in pore structure, this graph can be interpreted the following way. During the final stage the porosity exists as closed pores located on the grain boundaries. As the porosity increases the projected length of the pores will increase until the inception of the transition stage (≈5% porosity). At this point cylindrical pores start to form. During the transition stage the projected length will

gradually increase as the fraction of grain edges occupied by cylindrical porosity increases, until the pore structure enters the intermediate stage. At this point the grain edges are totally occupied by cylindrical porosity and the projected length becomes a constant value. Therefore, the projected length should equal the length of a grain edge. In order to verify this interpretation, the value for the projected length at the intermediate stage was set equal to the grain edge length. This value was inserted into an equation which relates grain size to edge length for a tetrakaidecahedron space filling geometry (GS = 2.785ℓ). This value was compared to grain size values obtained directly from the sites from which the values for the projected length were obtained. The values for the grain sizes were 2.23 μm and 2.26 μm, respectively, showing very good agreement between the two calculations and supporting the interpretation of this graph.

D. Experimental Verification of the Wingert Model

As discussed previously, the effects of pore and grain growth were incorporated into the Wingert Model by the factor Z_I. This factor can be determined experimentally by obtaining values for $\bar{r}$ and $\bar{G}$ as a function of porosity (see Table IV, Fig. 17), and substituted into the following equation:

$$Z_I = 0.0387\ (P/Y^2) \text{ where } Y = \bar{r}/\bar{G}$$

The values obtained from this investigation for Z_I are plotted in Figure 21 and are also listed in Table V to compare them to the values proposed by Wingert.

Wingert has assumed that Z_I remains constant during the transition stage at its value at the beginning of this stage. This is assumed because as cylindrical pores pinch off, instead of decreasing the fractional number of grain edges occupied by pores in the fraction of material exhibiting intermediate type behavior (alpha), it is assumed that the major effect in the transition stage is to isolate pores and, therefore, increase beta, the fraction of material exhibiting final stage behavior.

The experimental values obtained for Z_I are widely scattered from 0.36 → 0.87 (see Fig. 21 and Table V). In order to evaluate this data, attempts were made to fit a curve to these data. However, any curve that was tried exhibited a correlation coefficient showing that there was no trend to these data. Therefore, it was felt that an average value for Z_I should be obtained for the transition stage. The experimental value calculated was 0.54. It can be concluded that during the transition stage, on the average, the fraction of grain edges occupied by cylindrical porosity is 0.54.

This experimental result is in good agreement with that predicted by Wingert ($Z_I \approx 0.60$). Due to this agreement, the factor Z_I proposed by Wingert is believed to be a significant term necessary to be incorporated into the intermediate stage

sintering equation to correct for the modification of pore morphology.

E. Verification of the Zener Model

When a sufficient number of immobile particles are bound to a grain boundary, these particles can prevent its movement. The particle volume fraction (F) required to limit grain growth, as first stated by Zener,[29] is: $F = \frac{4}{3}\frac{r}{G}$ where r is the particle radius and G is the grain size. When this condition is fulfilled all but exaggerated grain growth will cease.

The behavior of many systems during sintering have also been assumed to obey this relationship, based on the underlying assumption of grain boundaries being pinned by immobile pores just as they are by immobile particles. Therefore, since the Zener relation states that $r/G = \frac{3}{4} P$, the results in Figure 17 are consistent with this behavior, and the figure shows that this relationship is followed through the entire sintering or hot-pressing process. We believe this result to be one of the few, if not only, experimental verifications of the Zener relationship.

The slope of the curve in Figure 17 is approximately equal to unity, in fairly close agreement with that expected from the Zener relationship. However, since the structure in the final stage is significantly different from the structure in the

intermediate stage, a change in slope might be expected from these two different microstructural conditions. Scatter in the data and the absence of data points at both ends of the transition region make it difficult to conclude if, in fact, there is any significant change in slope. An additional point about the transition region is that for a porosity level of about 10%, the value of the ratio $\bar{r}/\bar{G}$ is approximately 0.1. This value is consistent with that observed in many previously published sintering studies.

The microstructures observed in Figure 12 show all the pores to be at the grain boundaries; to some extent this is inconsistent with the Zener relation. The Zener relation is based on a homogeneous, as opposed to heterogeneous, distribution of particles or pores. Rosolowski and Burke[30] have derived separate expressions for these two extreme cases. For the case of a homogeneous distribution $F = \frac{4}{3}\frac{r}{G}$, while the relation $F = 8(\frac{r}{G})^2$ is obtained for a heterogeneous distribution of pores on grain boundaries. However, since these relationships have not been derived rigorously and the starting assumptions are simplistic, neither of these relationships may be applicable to real systems.

While the present work is concerned with the specific microstructure developed during pressure sintering, it appears that densification in a compact could conform to the Zener

relation under the condition of either hot-pressing or sintering. During hot-pressing, high stress is applied to the powder compact. This permits a higher densification rate and shorter times to reach full density. Due to these conditions, limited grain growth, as well as little pore coalescence is expected. Therefore, the number of pores is essentially constant and the decrease in r/G with decreasing porosity level is accomplished by a decrease in the mean pore radius. In contrast, during pressureless sintering, densification rates are typically lower and therefore longer times are needed to reach full density. The longer times permit more extensive grain growth and corresponding pore coalescence. Therefore, a decrease in r/G as porosity decreases is accomplished by a combination of increasing grain growth in the possible presence of an increasing mean pore radius due to Ostwald ripening. The behavior noted in Figure 17 is consistent with either interpretation.

The microstructural changes of grain growth, pore growth or these processes in combination have a significant effect on the densification rate. Wingert[1] has shown this in the form of a composite (Fig. 22) based on a number of different computer model outputs to show these effects on densification rate. Figure 22 indicates that if no grain growth or pore growth occurs, the predicted densification rates are quite high and a large discontinuity might be observed. Pore growth alone,

or grain growth and pore growth in combination, both tend to decrease the densification rate and contribute to a smoother transition between the various densification stages. Therefore, these processes have a significant effect on the densification rate and sintering models should be modified to incorporate these effects.

The verification of the Zener relationship agrees with the criticism[31] aimed at the Coble model for not taking into account pore growth. Conversely, the assumptions made in the development of the model by Rosolowski and Greskovich[11] are proven through our experimental findings. In addition, the statistical model proposed by Kuczynski[9] is in agreement with the present proof of the Zener relationship. The incorporation of the results of this investigation into the microstructural modification model developed by Wingert[1] proves the validity of that author's model. Even though the Wingert model uses a simplistic geometry, it takes into account the effects of a changing microstructure. This shows that even though a simple geometry may be inaccurate, a model can be modified to take into account a changing pore and grain structure, and obtain qualitative expressions to model the sintering process.

The present observations, that $r/G \sim P$ for hot-pressed CoO (Fig. 17) were presented at the 1979 American Ceramic Society convention and at the Fifth International Conference on Sintering and Related Phenomena (June 18-20, 1979) and will be published in the proceedings of the latter mentioned conference. At the same conference a paper was presented by Uskokovic, et al.[33] that showed preliminary survey results but indicated a similar relationship to be observed for a number of other ceramic oxide systems including NaF, Nb_2O_5, UO_2, MgO and ZnO. In addition, Aigeltinger and Drolet[34] in studies on Carbonyl iron powder presented results similar to those obtained in this investigation. Specifically, these investigations demonstrated that the mean grain intercept($\bar{D}$) was linearly related to the ratio of the mean pore intercept length to pore volume fraction ($\bar{\lambda}/P$) throughout the entire sintering range studied. In this latter work, pores in the carbonyl iron are distributed homogeneiously (i.e. pores) both at grain boundaries and within the grains) while in the present CoO work pores are distributed heterogeneously (i.e. only at grain boundaries). Thus it seems that the Zener relation holds for a wide variety of both ceramic and metallic materials.

V. SUMMARY

The use of density measurements and quantitative image analysis are good tools to study the microstructural development in pressure sintered CoO. Density measurements provided values for the variation in porosity on the macroscopic level while qualitative image analysis allowed examination on the microstructural level.

In order to examine the variation in open and closed porosity a combination of macroscopic density measurements and measurements on the microstructural level of the mean projected length of pores were used. These results followed previously predicted behavior.[21,28] The measurement of the mean projected length of pores vs. porosity (Fig. 20) was a good parameter to quantitatively describe the transition from closed porosity to open cylindrical porosity. The grain size obtained from the measurement of the mean projected pore length agreed well with those obtained from measurement by the linear intercept technique.

Quantitative image analysis provided information on how the number of pore/unit volume vs. pore diameter varied with porosity (Figs. 18 and 19). The general trend was for the number and size of the pores to decrease as the material densified. In addition, quantitative image analysis provided considerable information on how the pore radius varied as a function

of total porosity. Combination of these results with grain size determination led to the experimental verification of the Zener relationship. This verification of the Zener relationship proves its applicability to the sintering process.

Finally, the automatic system developed for performing quantitative image analysis provides a fast and accurate method for studying the modification of pore morphology. The major advantage arises from the ability to alter grey levels between pore and matrix for optimum detectability.

TABLE I

Pressure Sintering Conditions for CoO

Sample #	Temp (°K)	Pressure (MPa)	Time (min.)	(g/cc) Density*	% Theoretical
3-JM-S	1423	86.2	69	6.258	97.22
4-JM-S	1423	86.2	8	5.809	90.25
				5.619	87.29
5-JM-S	1323	86.2	3	5.150	80.01
				5.092	79.10
				5.000	77.78
6-JM-S	1323	86.2	4	5.478	85.10
				5.424	84.26
				5.599	86.98
7-JM-S	1323	86.2	5.5	5.550	86.19
				5.450	84.69
				5.570	86.48

*Liquid displacement technique; more than one value appears because different parts of the specimen were measured.

TABLE II

Comparison of Porosity Between Millipore and Liquid Displacement Technique

#7 JM-S	Millipore	Liquid Disp.	#4 JM-S	Millipore	Liquid Disp.
17.39%			5.61		
13.40%			5.60		
11.47%			7.80		
16.62%	15.00%	14.20%	10.23	6.67%	9.75%
16.63%			7.50		
14.47%			3.26		

#3 JM-S			#5 JM-S		
.17			11.13		
1.16			18.46		
1.34			11.42		
1.55			12.47	15.70%	21.62%
5.23			21.34		
6.78			17.03		
3.93			19.83		
3.64	3.46%	2.78%	13.92		
7.43					
3.99					
2.92					
5.21					
2.16					
2.18					

TABLE III

Porosity	d, Pore Size (μm)	G, Grain Size (μm)	r/G
.87	.345	5.50	.03
1.16	.501	8.18	.03
1.34	.634	13.34	.02
2.16	.447	7.08	.03
2.18	.576	11.30	.03
2.92	.759	9.50	.04
3.26	.920	8.94	.05
3.64		9.63	
3.93	.815	8.04	.05
5.60	.817	7.54	.05
5.61	.907	7.10	.06
6.60		7.05	
6.78		9.12	
7.50	.903	4.93	.09
7.80	.922	5.69	.08
10.23	.886	4.40	.10
11.13	.445	2.91	.08
11.42	.576	2.82	.10
11.47	.584	3.35	.09
12.47	.444	2.41	.09
13.46	.702	3.13	.11
13.92	.637	2.94	.11
14.47	.878	2.53	.17
16.62	.864	2.45	.17
16.63	.809	2.58	.16
17.03	1.017	2.81	.18
17.39	.836	2.22	.19
18.64		2.10	
19.83	.608	1.87	.18
21.34	1.121	2.30	.24

TABLE IV

Conversion Factors from πMC Units to Microns* on SEM

800X	Y = πMC units	X = Microns
	$X = \frac{Y}{1.92}$	
1600X	$X = \frac{Y}{4}$	
2000X	$X = \frac{Y}{5}$	
4000X	$X = \frac{Y}{10.53}$	

Calibrated at tilt angle of 30° and working distance of 11 mm.

* These conversion factors are obtained by imaging a copper grid of known size and measuring the grid in πMC units.

TABLE V

COMPARISON OF EXPERIMENTAL DATA TO WINGERT MODEL

POROSITY	Z_I EXPERIMENTAL	Z_I WINGERT
5.60	0.87	0.60
5.61	0.60	0.60
7.50	0.36	0.60
7.80	0.47	0.60
10.23	0.39	0.60
11.13	0.67	0.60
11.42	0.44	0.60
12.47	0.60	0.60
13.46	0.43	0.60
	AVE. = 0.54	AVE. = 0.60

$$Z_I = 0.0387 \ (P/Y^2)$$

where: $Y = \bar{r}/\bar{G}$

Z_I = FRACTION OF GRAIN EDGES OCCUPIED BY A CYLINDRICAL PORE DURING THE INTERMEDIATE STAGE.

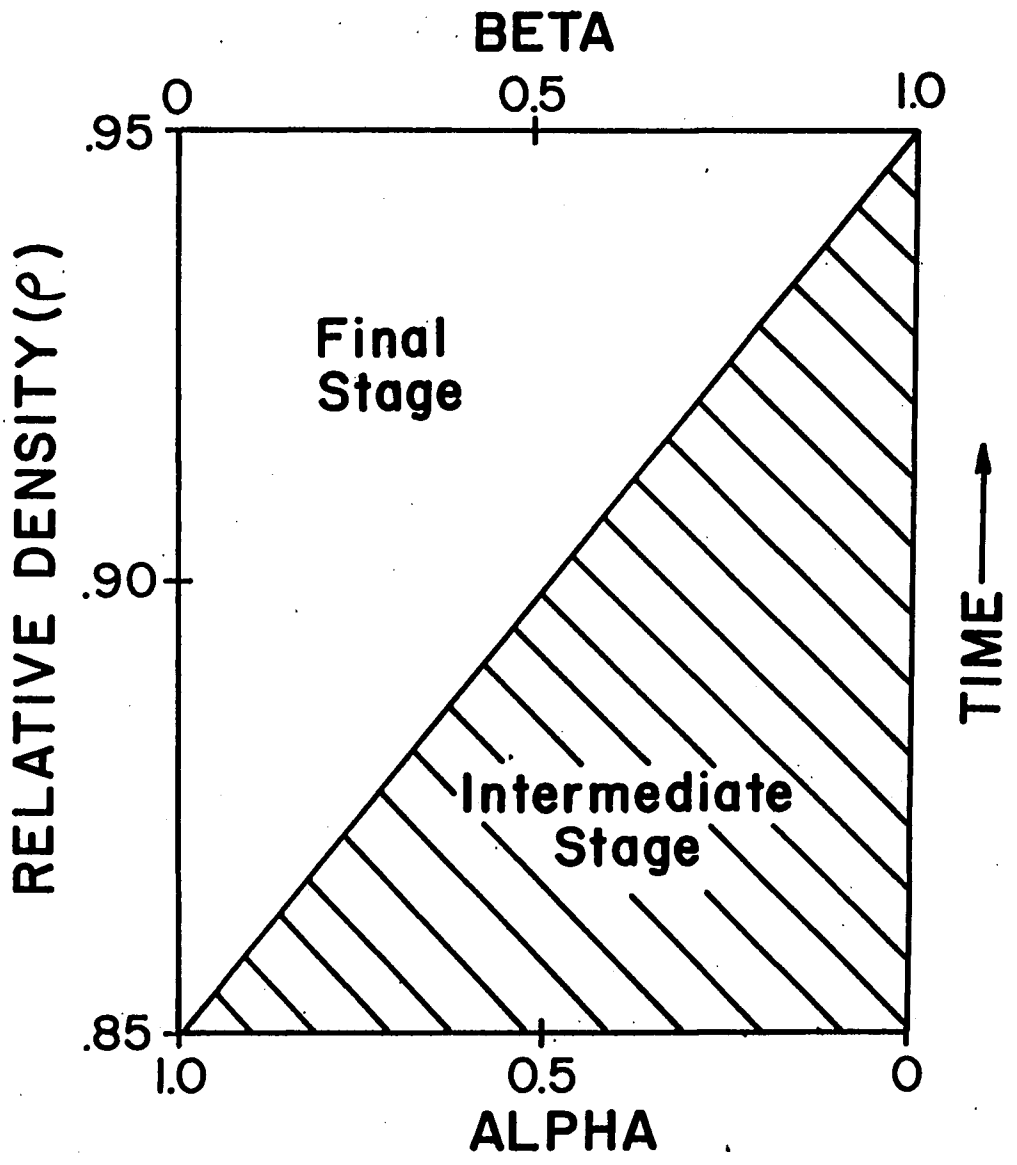

Figure 1. Schematic Representing the Gradual Shift from Intermediate to Final Stage Pore-Grain Structure During the Transition Stage.

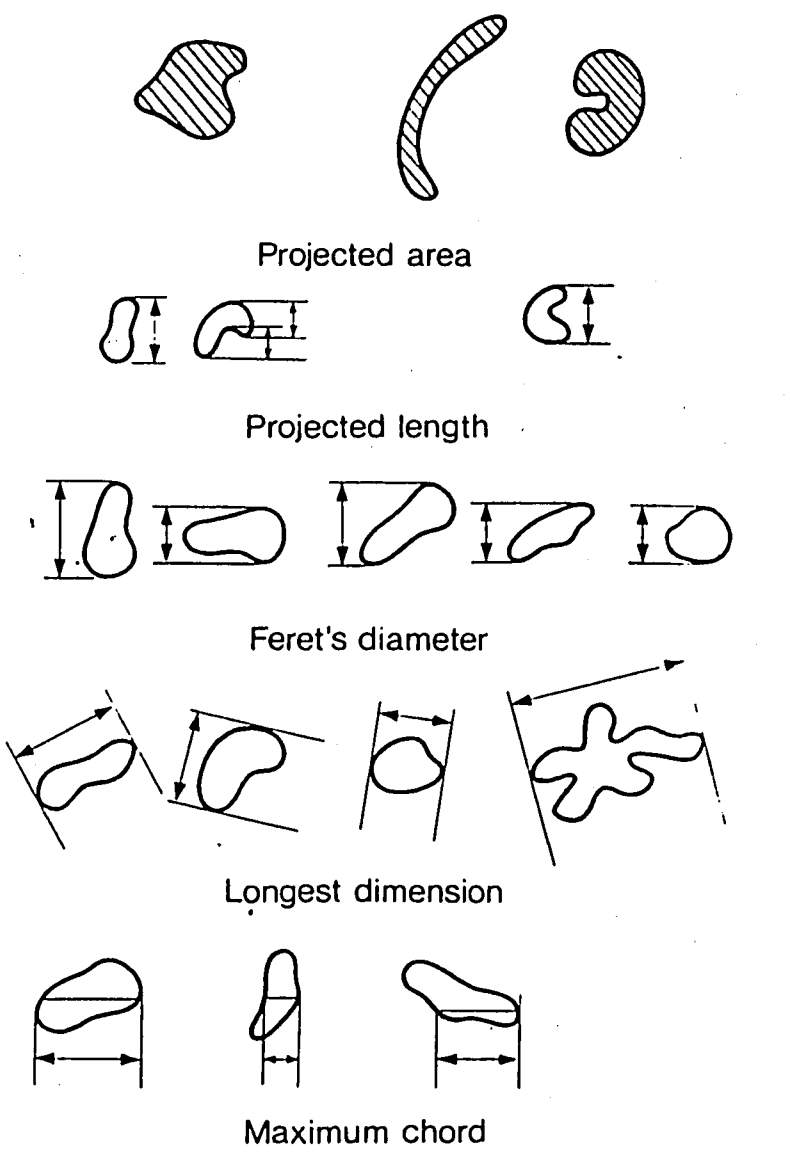

Figure 2. Measurement parameters for characterization of particles by πMC.

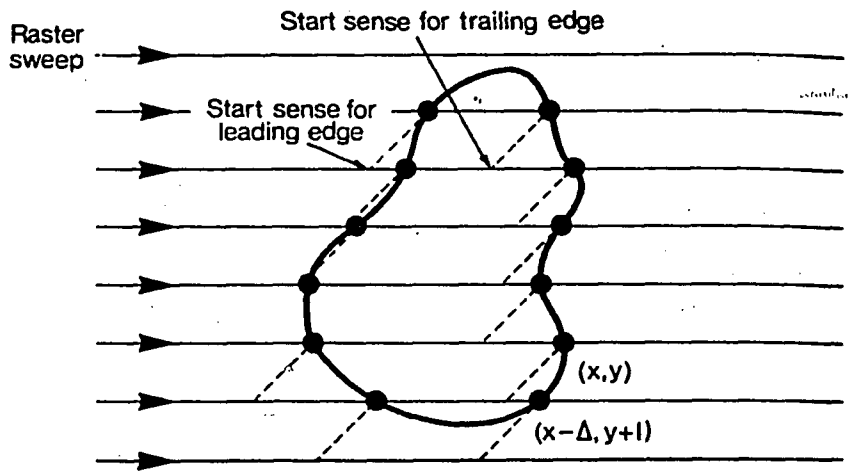

Figure 3. Schematic showing detection of particle boundaries by πMC.

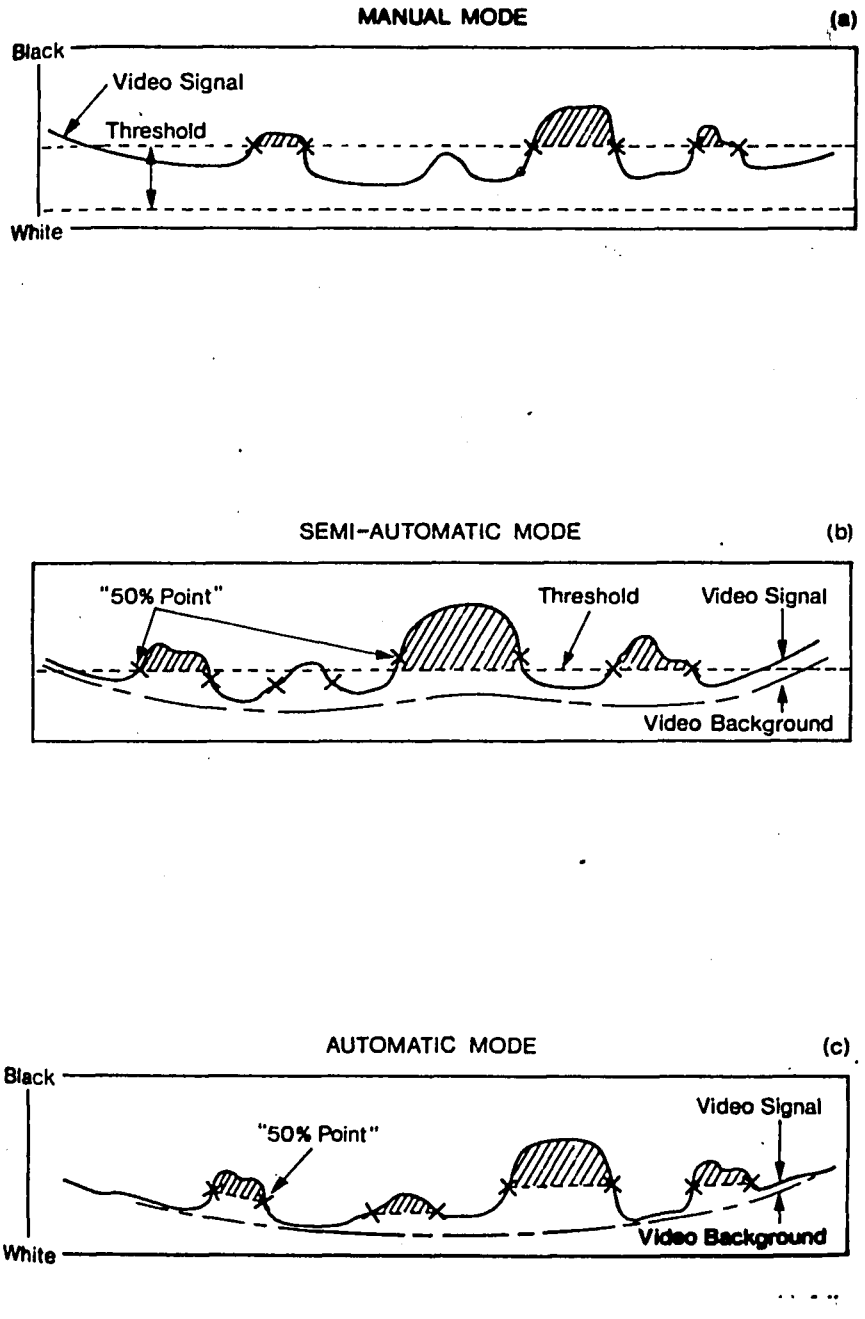

Figure 4. Schematic showing threshold detection modes of operation - (a) manual; (b) semi-automatic; (c) fully automatic.

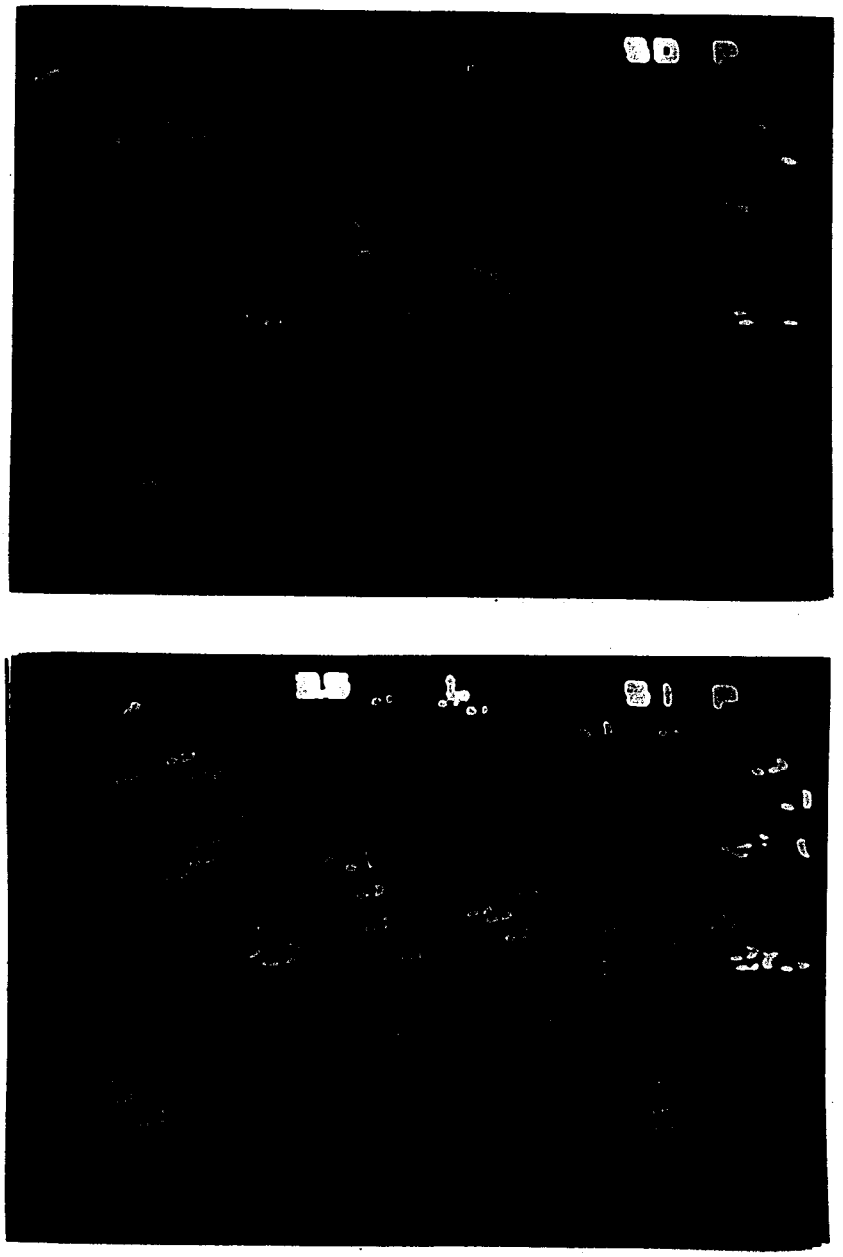

Figure 5. Pictures of TV monitor showing (a) tagging of pores; (b) outlining of pores.

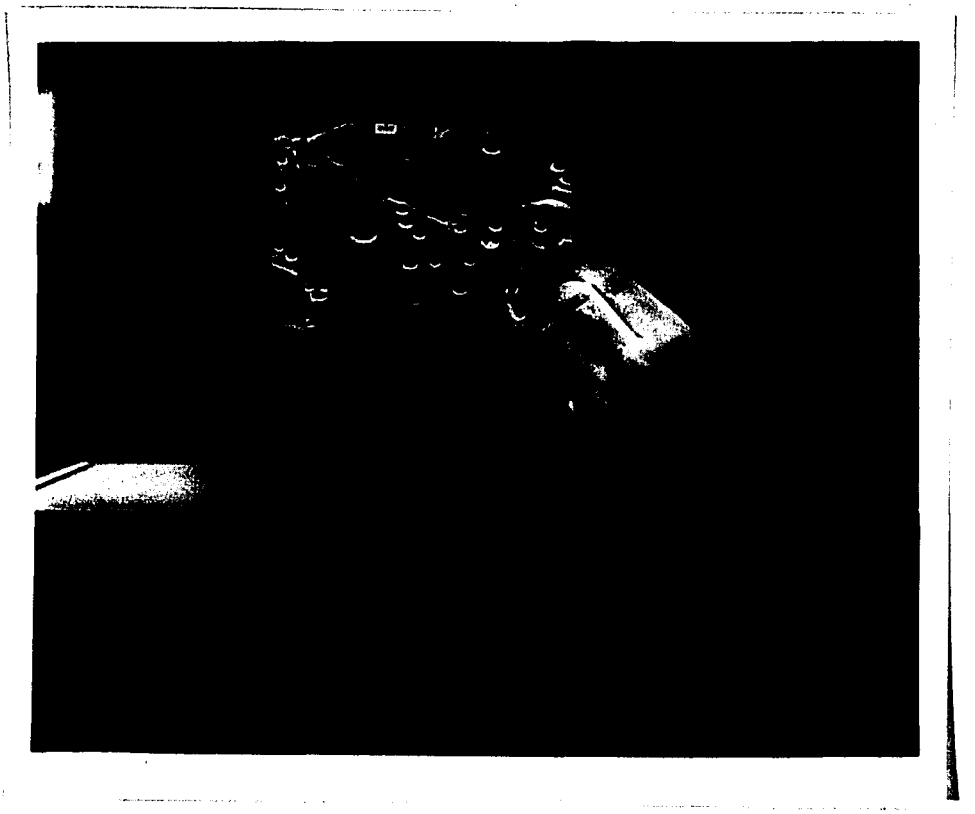

Figure 6. Picture showing utilization of the light pen.

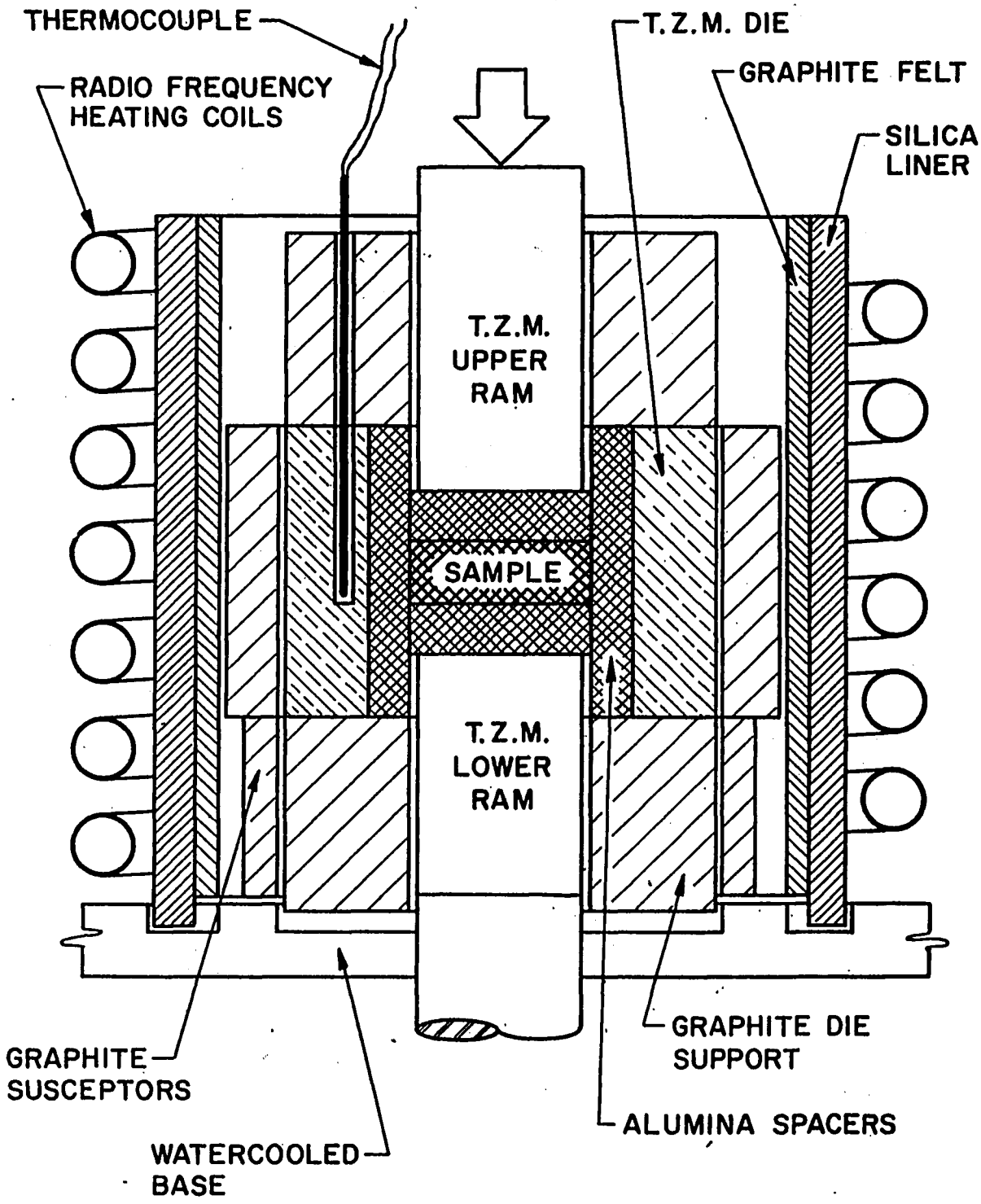

Figure 7. Hot Pressing Die Assembly.

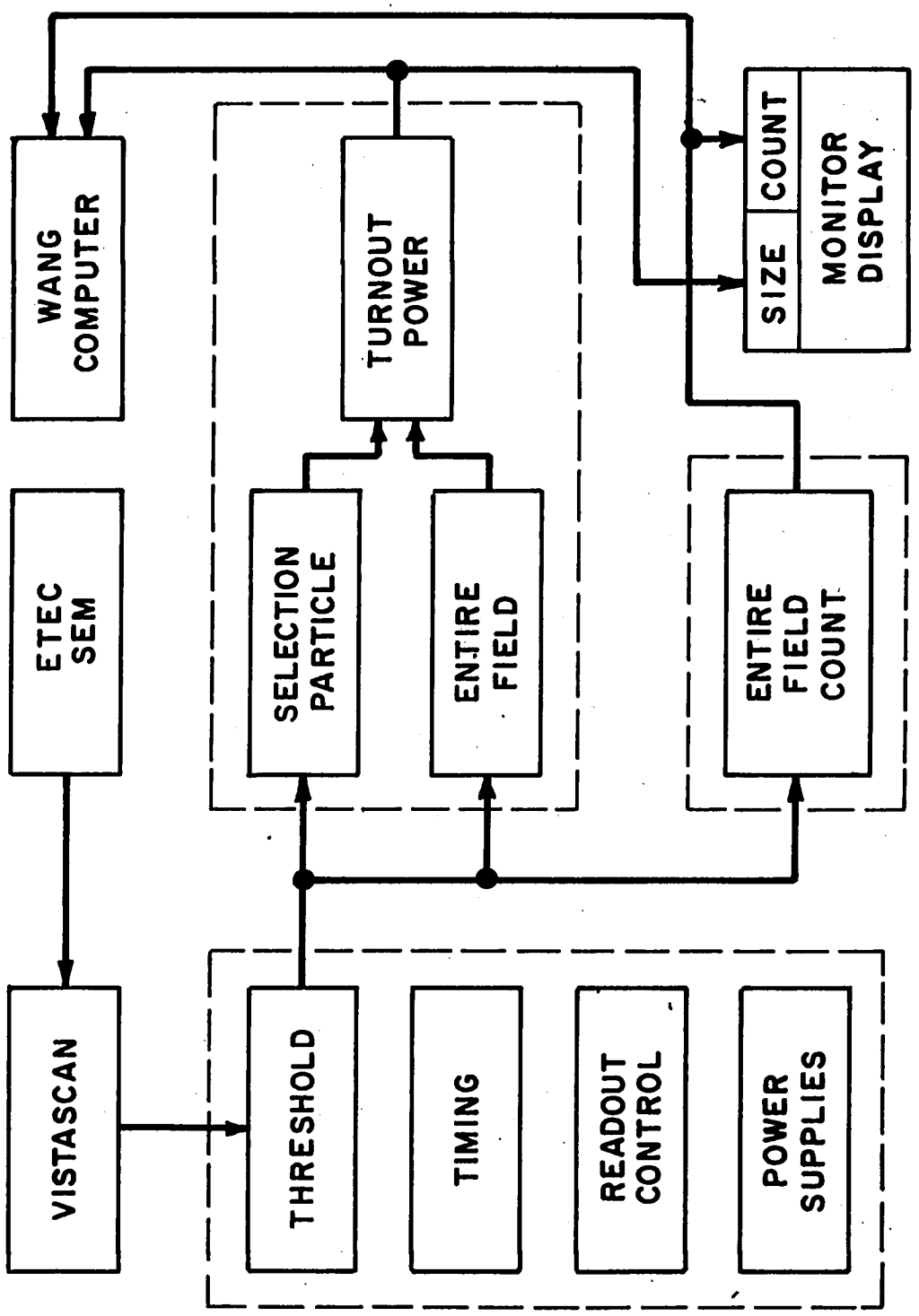

Figure 8. Schematic representing equipment used for Quantitative Image Analysis.

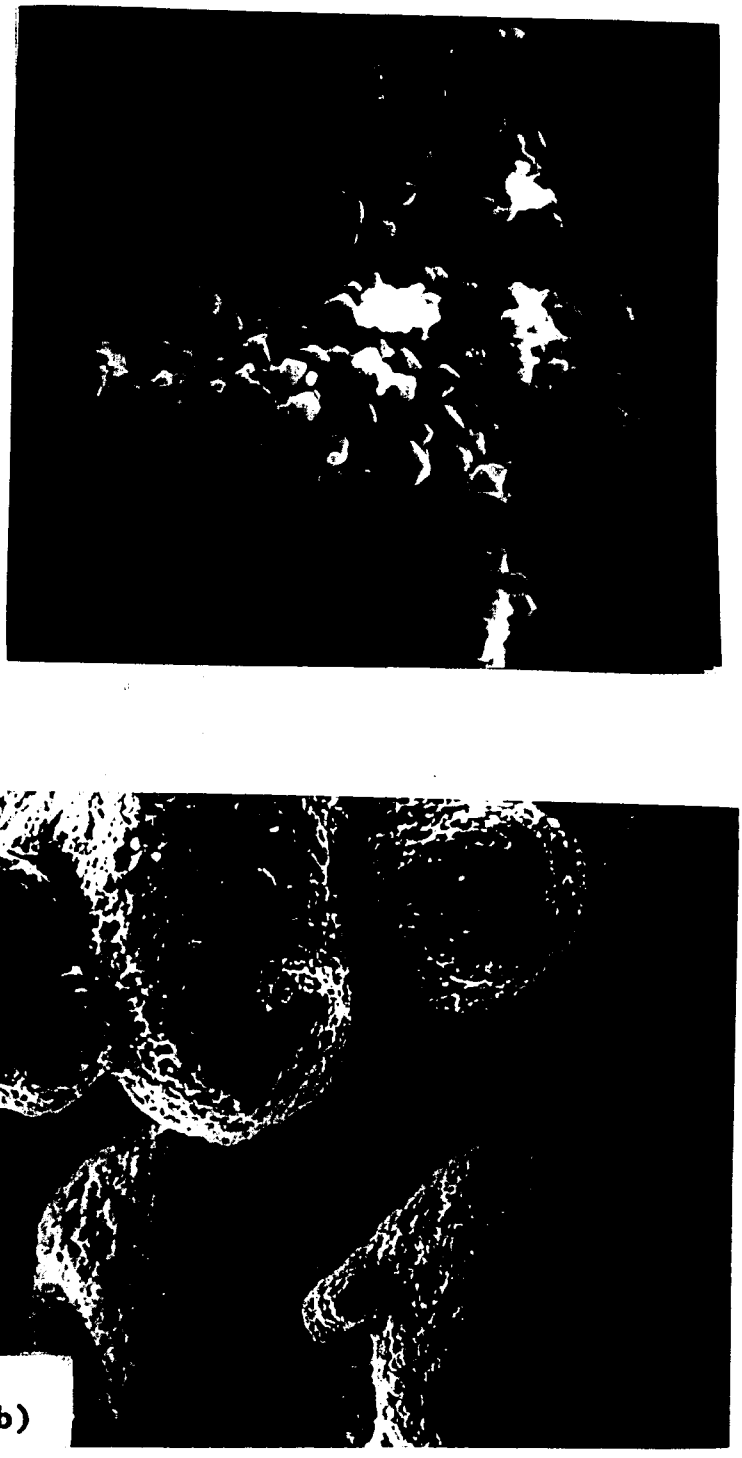

Figure 9. SEM micrographs of CoO powder - (a) Batch 1; (b) Batch 2.

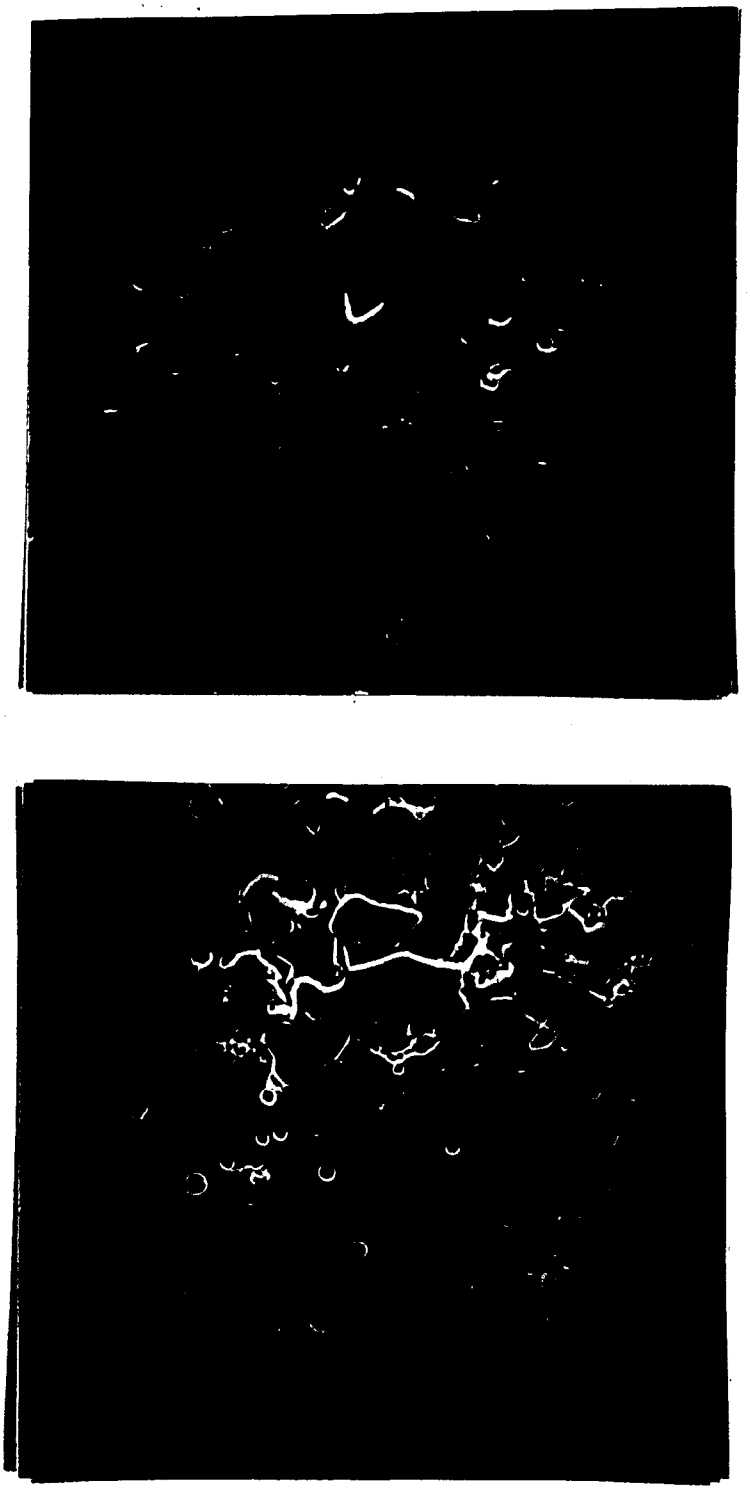

Figure 10. SEM micrographs of resulting microstructure from (a) Batch 1; (b) Batch 2.

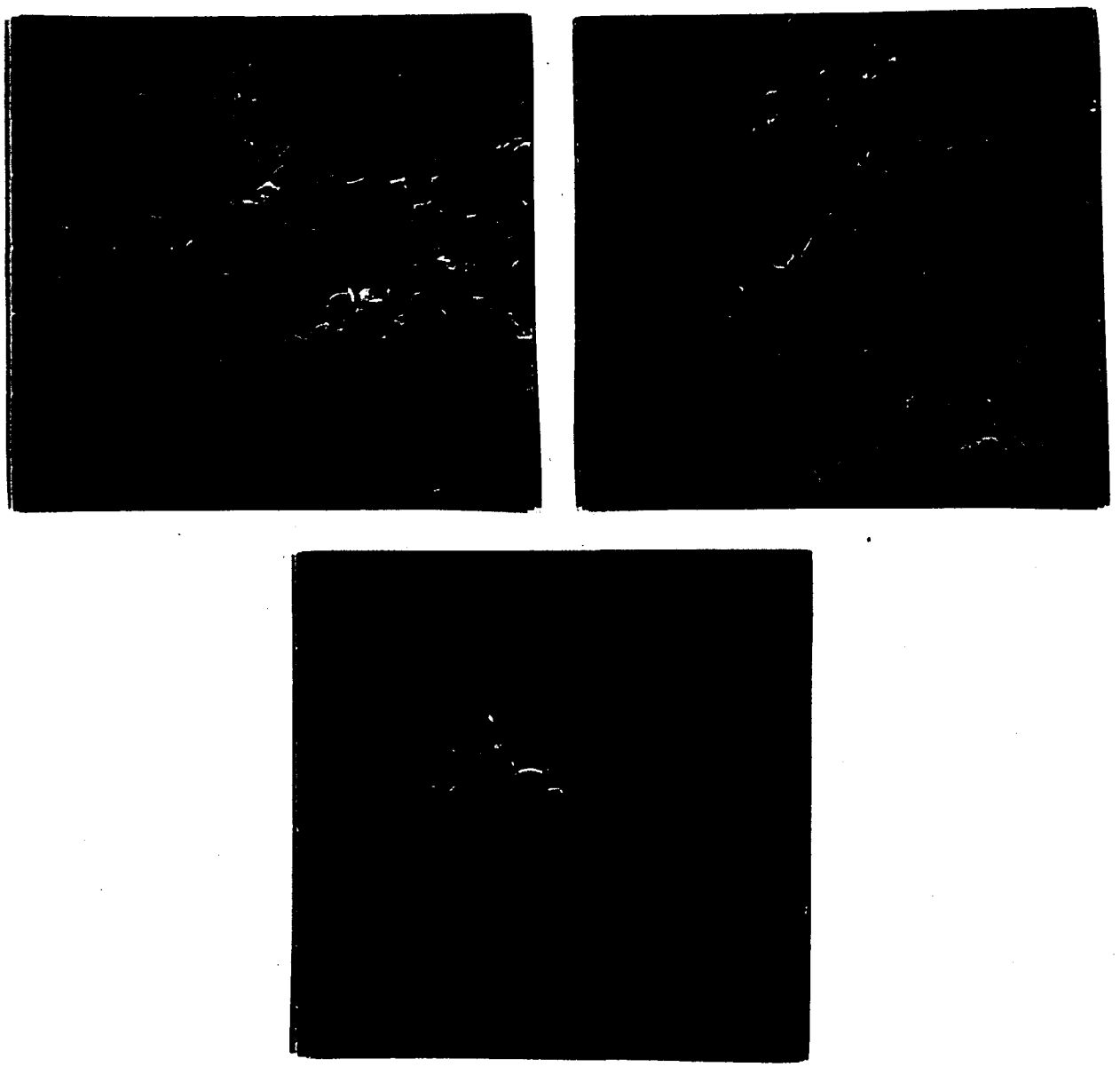

Figure 11. SEM micrographs of low density CoO specimen showing decreasing pore area and density gradient.

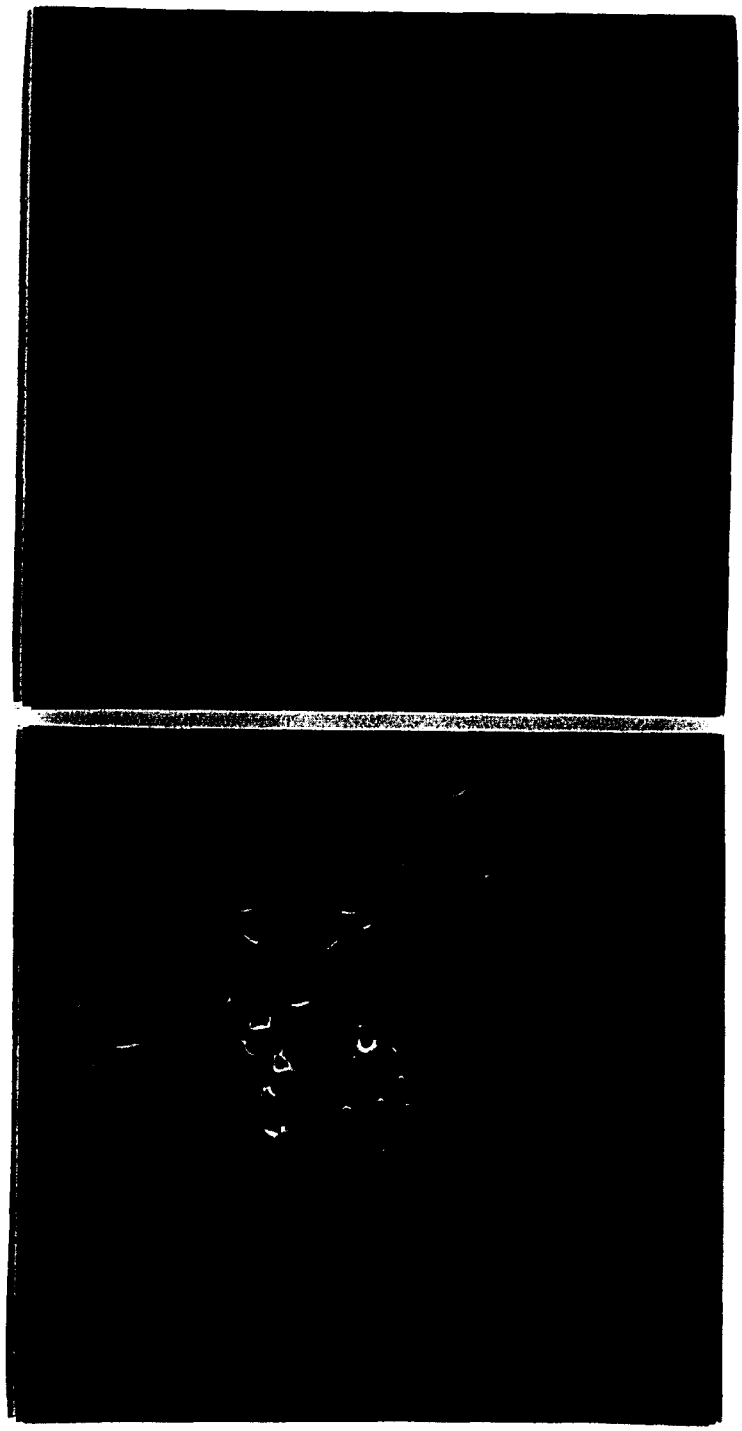

Figure 12. SEM micrographs representing shift from transition to final stage - (a) 6% porosity; (b) 3% porosity.

Figure 13. SEM micrograph of typical microstructure of a high density specimen of CoO.

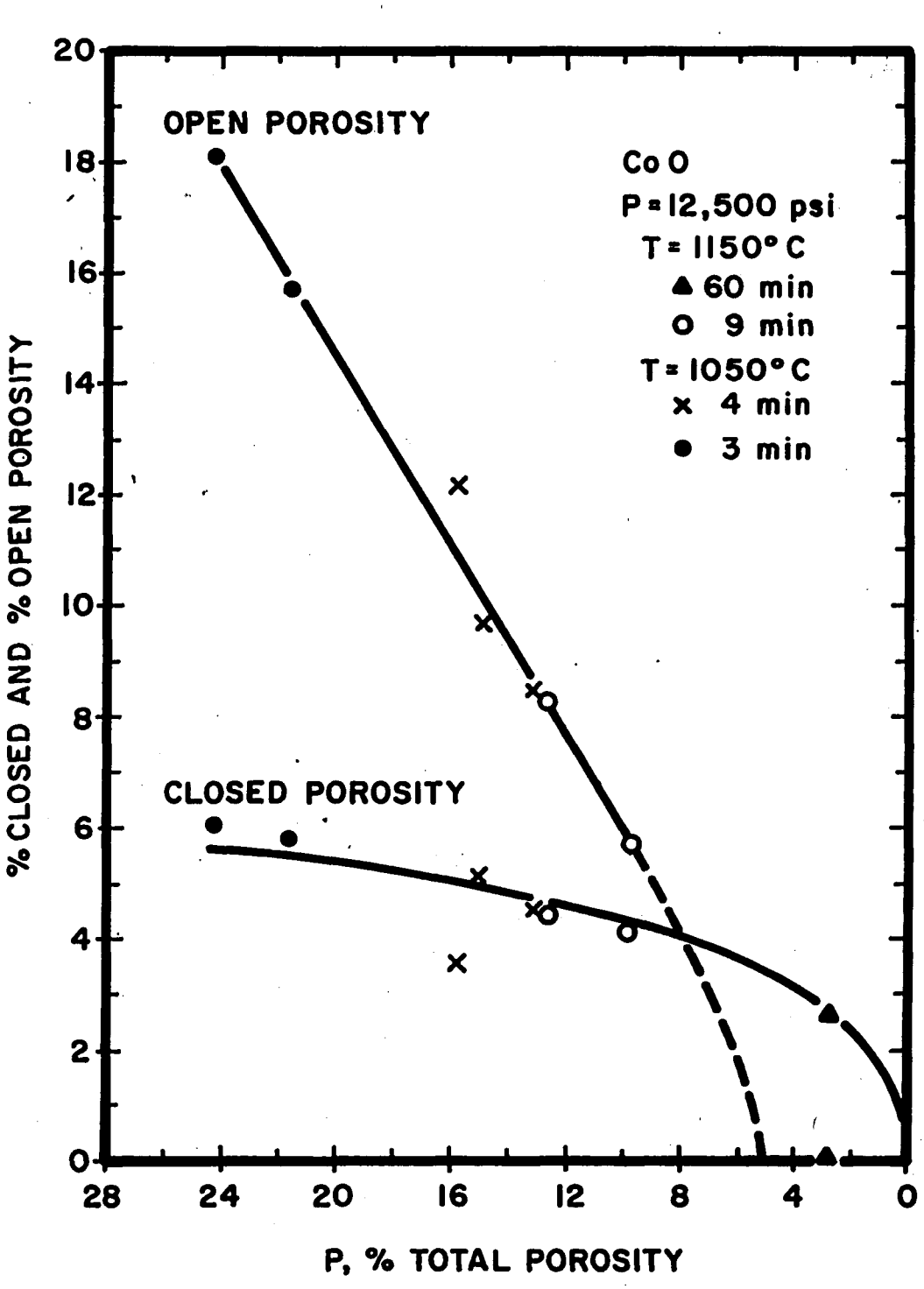

Figure 14. Porosity curves showing variation in open and closed porosity as a function of porosity.

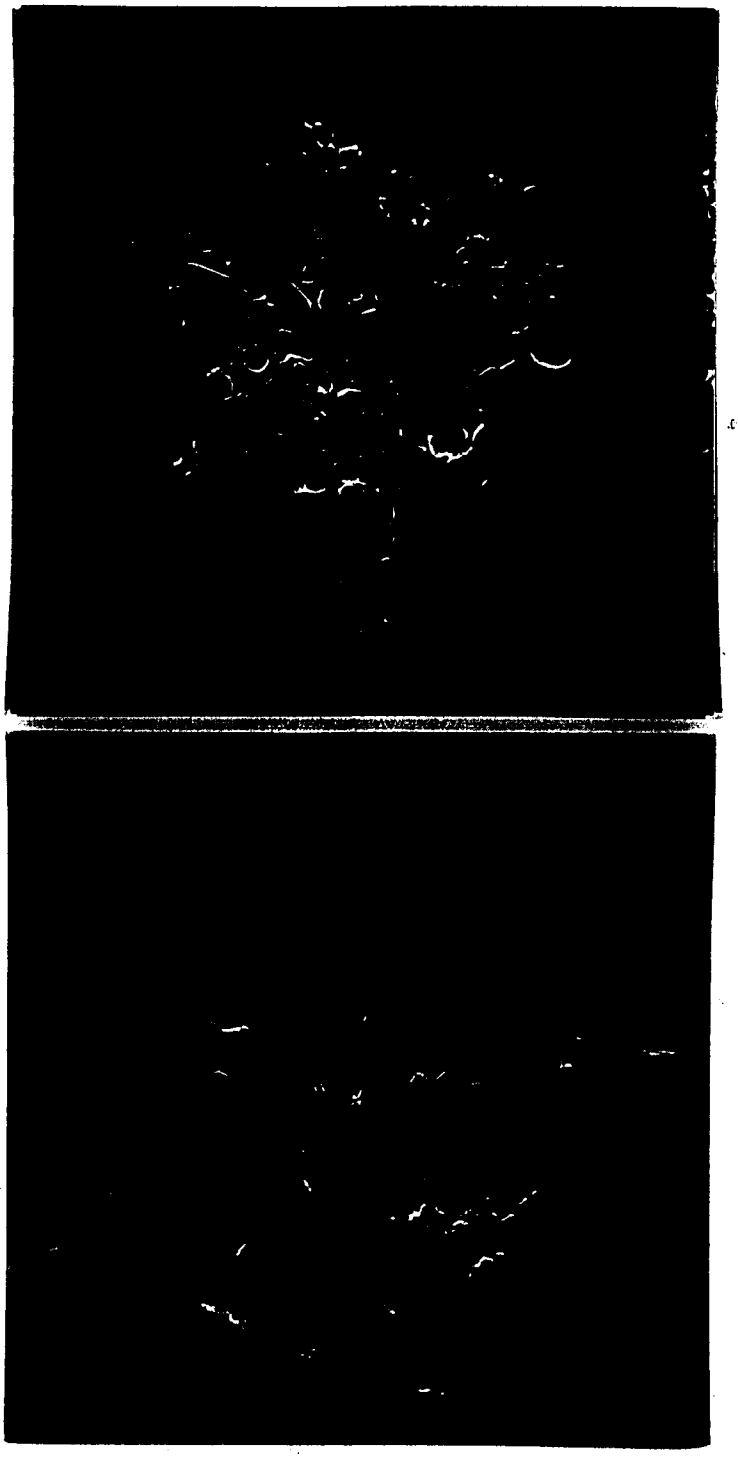

Figure 15. SEM micrographs representing internal porosity in (a) polished surface; (b) fracture surface.

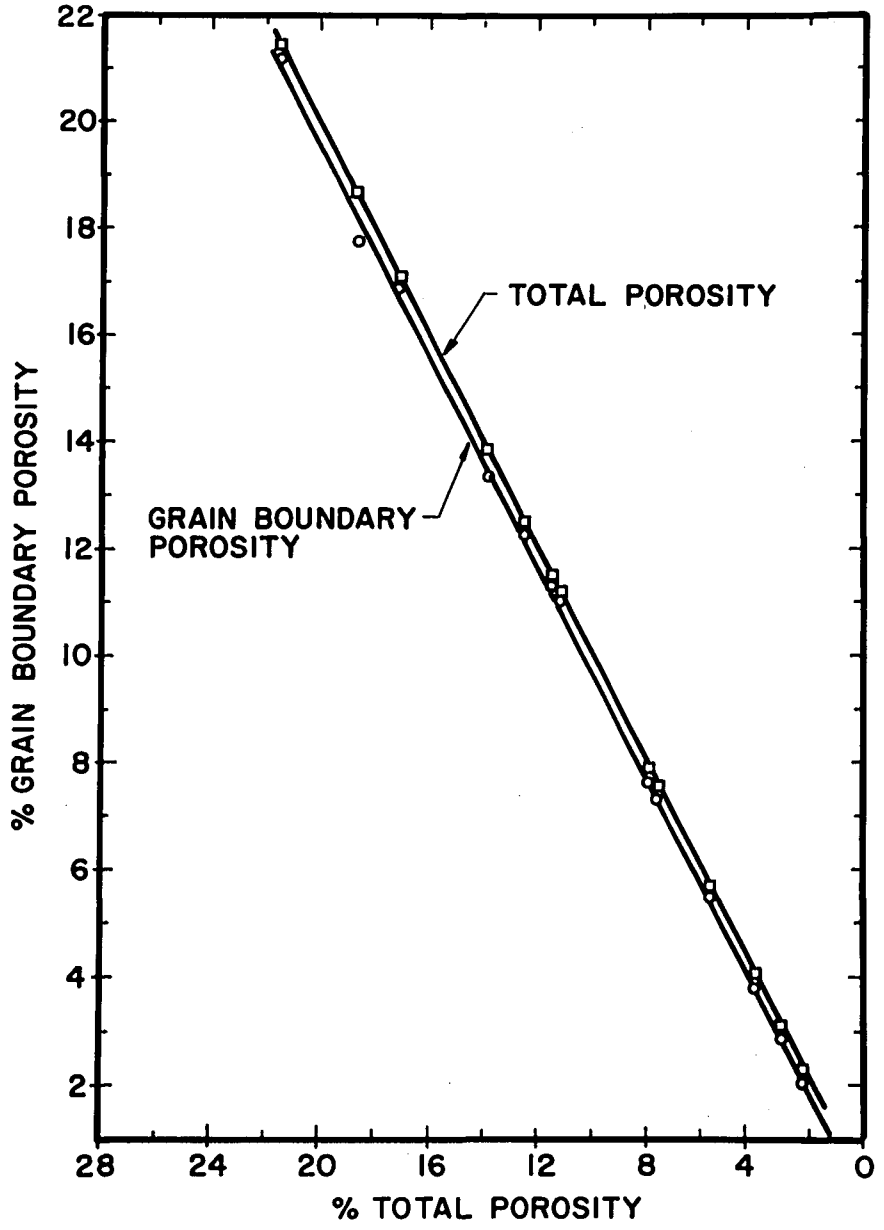

Figure 16. Curves representing amount of internal porosity.

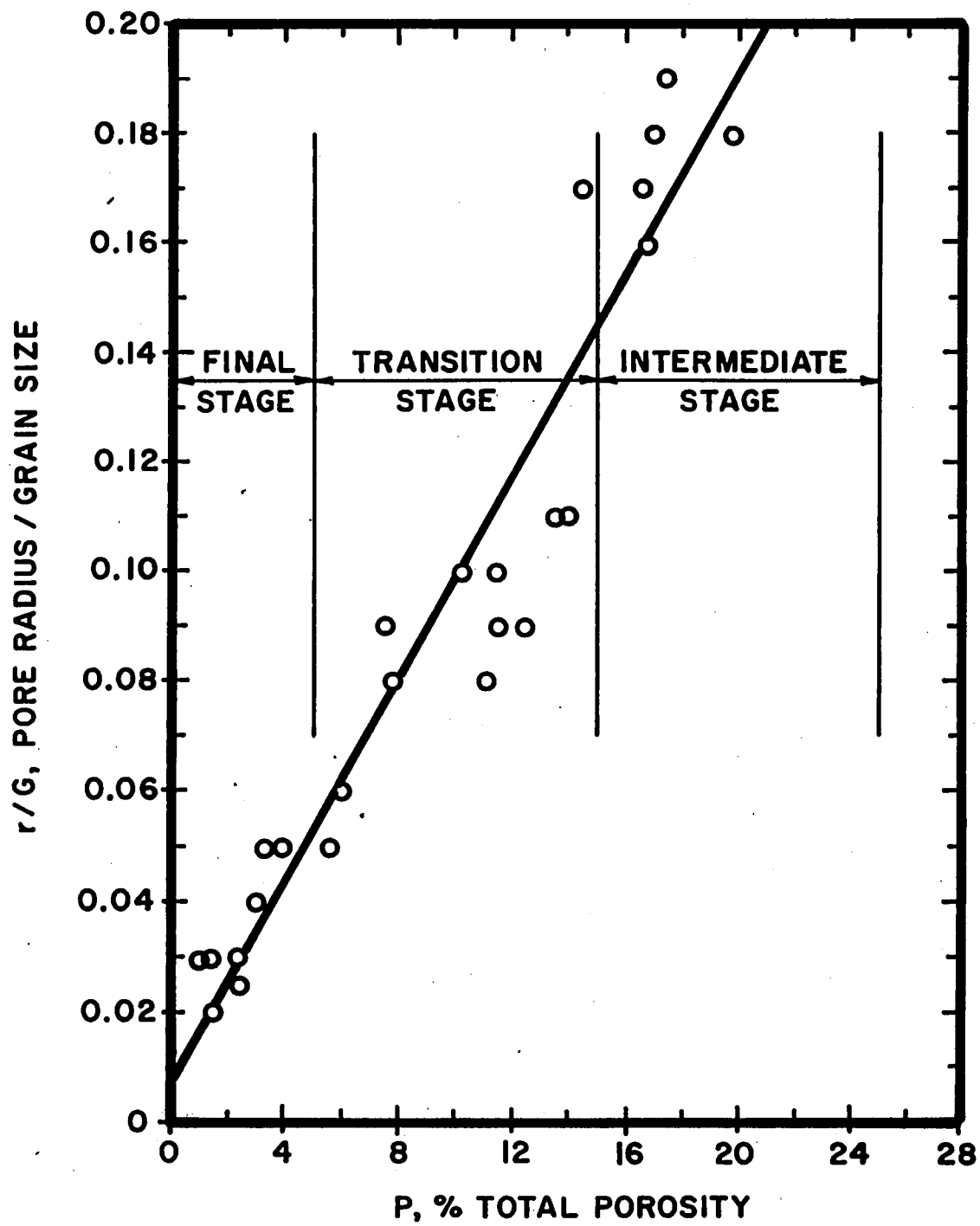

Figure 17. Plot of r/G vs. total porosity.

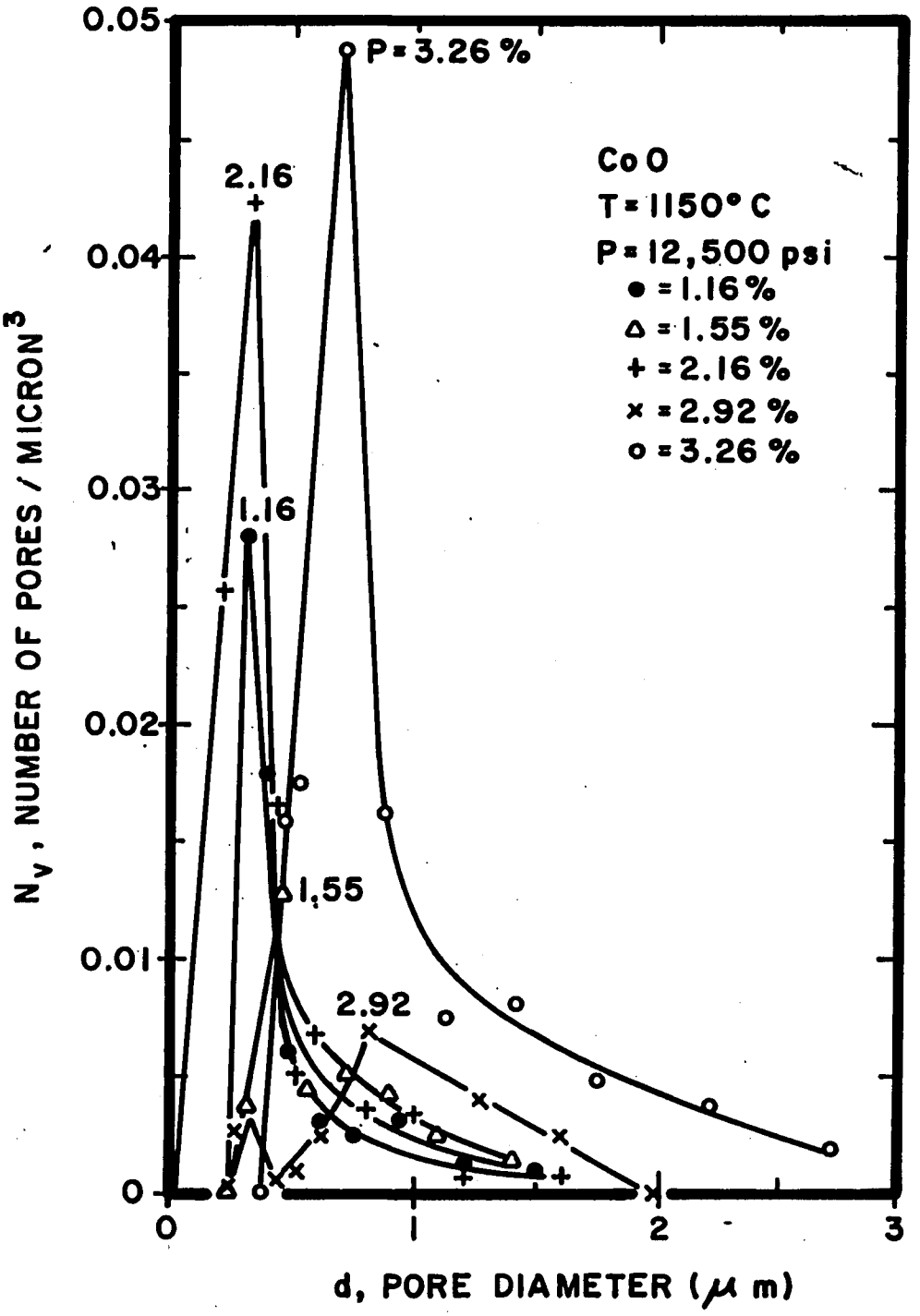

Figure 18. Plot of N_V vs. pore diameter.

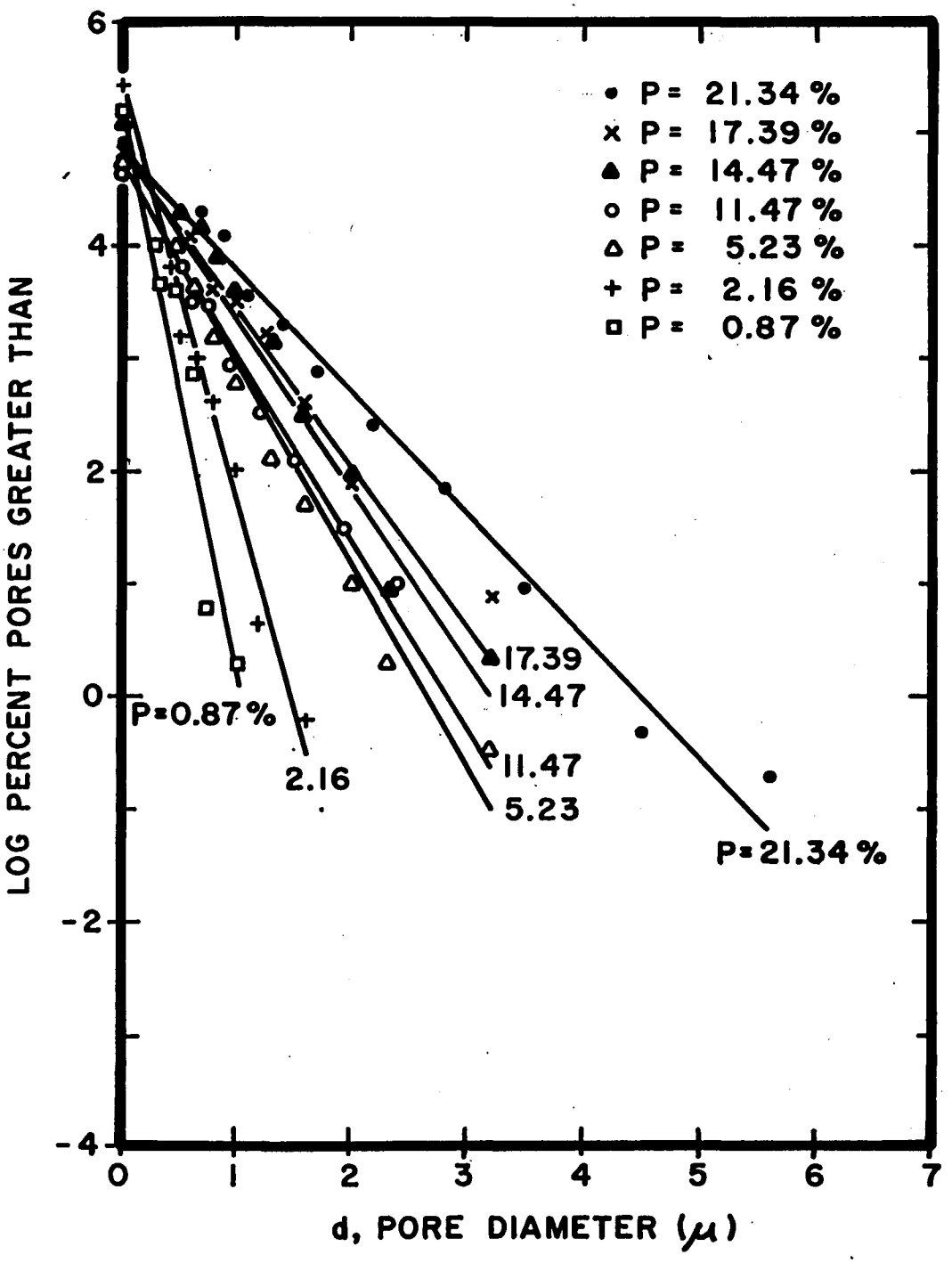

Figure 19. Plot of log pct. pores greater than vs. pore diameter.

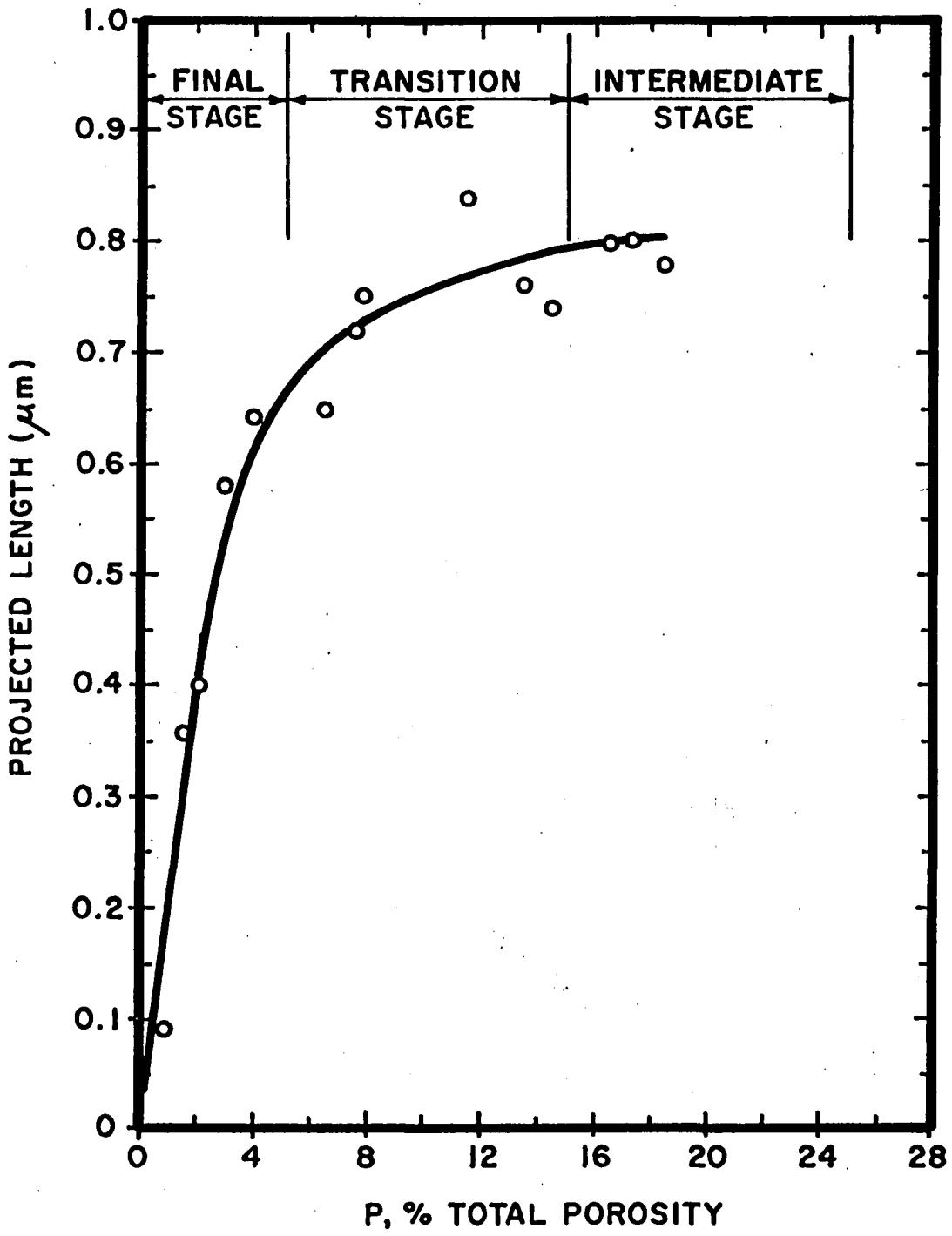

Figure 20. Plot of mean projected length vs. total porosity.

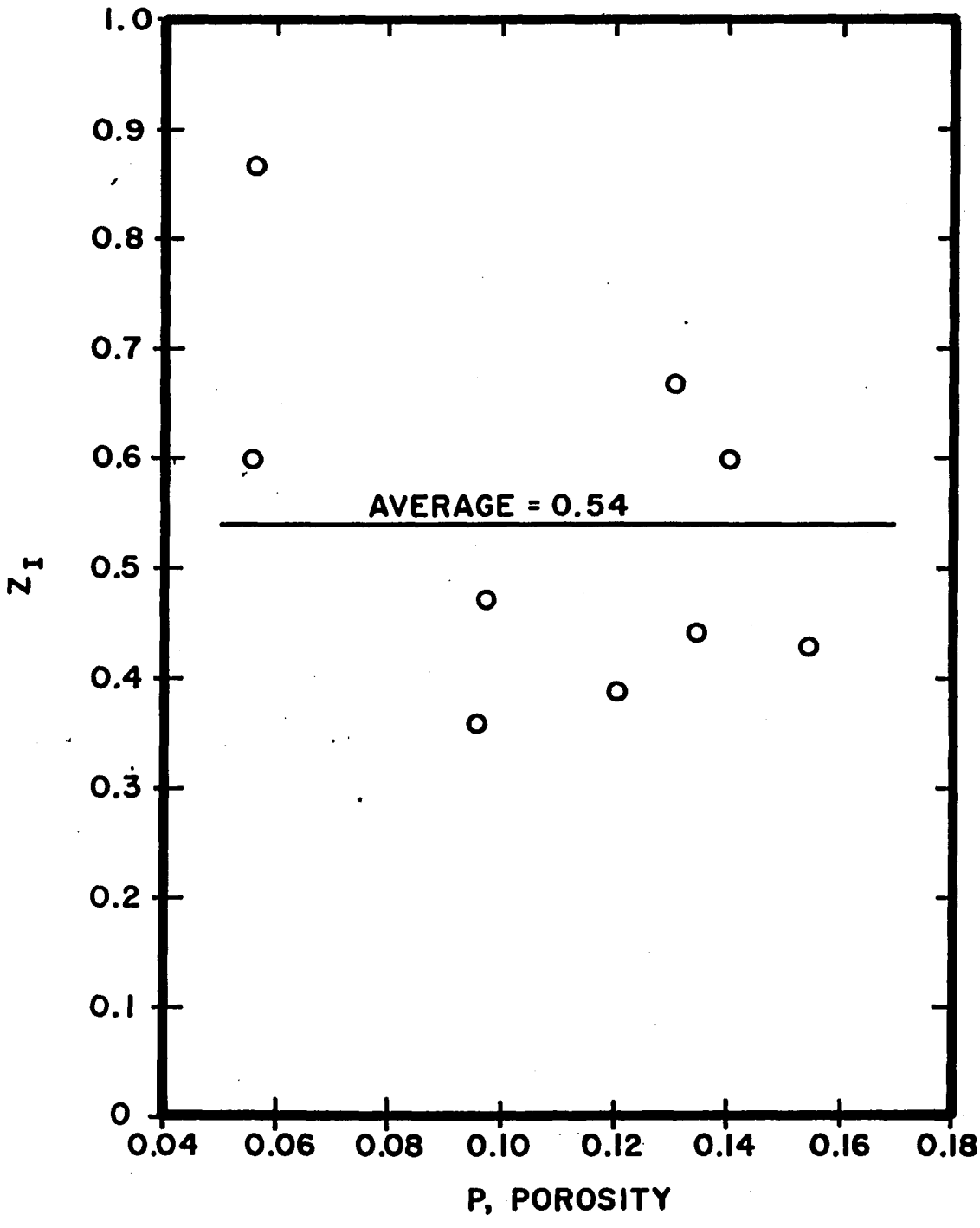

Figure 21. Plot of Z_I vs. total porosity.

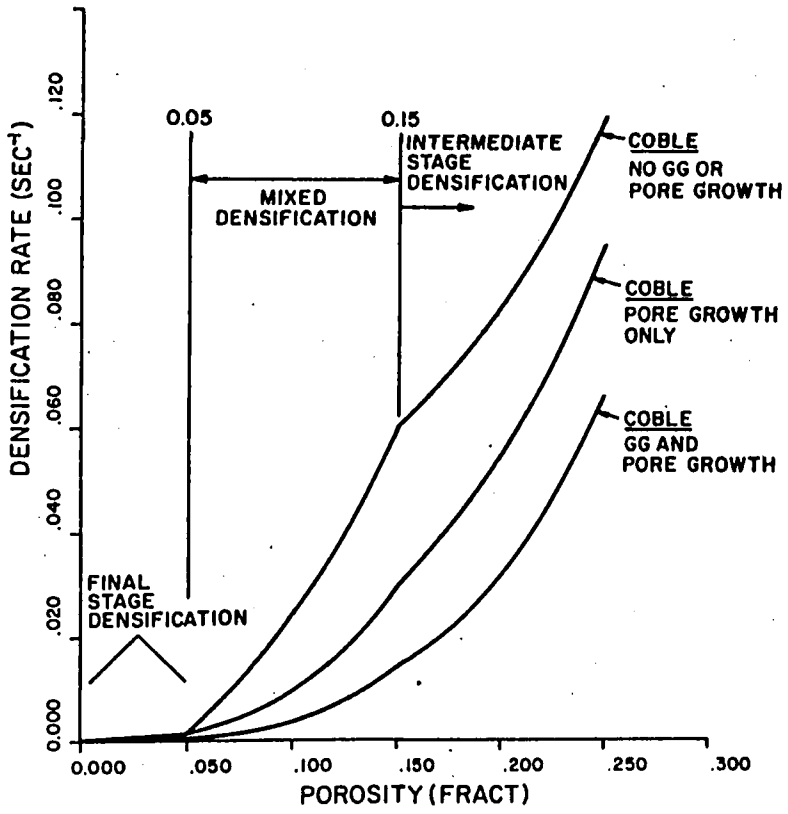

Figure 22. Densification Rate vs. Porosity Curves Showing Effect of Pore Growth Then Pore Growth and Grain Growth Considerations.

REFERENCES

1. P. Wingert, "The Study and Modeling of the Mechanisms Contributing to Densification During the Intermediate and Final Stages of Pressure Sintering", M.S. Thesis, Lehigh University (1977).
2. G. Arthur, "Porosity and Permeability Changes During the Sintering of Copper Powder", J. of Inst. Met., 83, 329 (1954-55).
3. S. C. Coleman and W. B. Beere, "The Sintering of Open and Closed Porosity in UO_2", Phil. Mag., 31 [8] 1403 (1979).
4. D. B. Budworth, "Theory of Pore Closure During Sintering", Trans. Amer. Ceram. Soc., 69 [1] 29 (1970).
5. R. L. Coble, "Sintering Crystalline Solids I - Intermediate and Final Stage Diffusion Models", J. App. Phys., 32 [5] 787 (1961).
6. R. L. Coble and T.K.Gupta, "Intermediate Stage Sintering", p. 433 Sintering and Related Phenomena, ed. Kuczynski et al., Gordon and Breach, New York (1967).
7. W. Beere, "The Intermediate Stage of Sintering", p. 149-155 in Vacancies '76, The Metals Society, London (1976).
8. R. L. Eadie and G. C. Weatherly, "Contributions of Grain Boundary and Volume Diffusion to Shrinkage Rate During Sintering" p. 239-248 in Sintering & Catalysis, G. Kuczynski ed. Materials Science Research, Vol. 10, Plenum Press 1975.
9. G. C. Kuczynski, "Statistical Theory of Pore Shrinkage and

Grain Growth During Powder Compact Densification", p. 235 Ceramic Microstructures '76, ed. R. M. Fulrath and J. A. Pask, Westview Press (1977).

10. D. L. Johnson, "A General Model for the Intermediate Stage of Sintering", J. Amer. Ceram. Soc., 53 [10] 574 (1970).
11. J. H. Rosolowski and C. Greskovich, "Theory of the Dependence of Densification on Grain Growth During Intermediate Stage Sintering", J. Amer. Ceram. Soc., 58 [5-6] 177 (1975).
12. T. K. Gupta, "Possible Correlation Between Density and Grain Size During Sintering", J. Amer. Ceram. Soc., 55 [5] 276 (1972).
13. S. C. Samanta and R. L. Coble, "Correlation of Grain Size and Density During Intermediate Stage Sintering of Ag", J. Amer. Ceram. Soc., 55 [11] 583 (1972).
14. E. M. C. Huijser-Gerits and G. D. Rieck, "Changes in Microstructure of Oriented Ba_3 Co_2 Fe_{24} O_{41} Material During Sintering. I.", J. Appl. Cryst., 7 474 (1974).
15. P. Kumar and D. L. Johnson, "Sintering of CoO: Intermediate Stage", J. Amer. Ceram. Soc., 57 [2] 65 (1974).
16. P. Wingert and M. R. Notis, "Densification Mapping for the Intermediate and Final Stages of Hot-Pressing", unpublished paper, Lehigh University (1977).
17. J. F. C. Brown, "Automatic Microscopic Analysis with the πMC Particle Measurement Computer", Microscope, 19, 285 (1971).
18. W. K. Chen and R. A. Jackson, "Oxygen Self-Diffusion in

Undoped and Doped Cobaltous Oxide", J. Phys. Chem. Sol., 30 [6] 1309 (1969).

19. V. Krishnamachari and M. R. Notis, "High Temperature Deformation of Polycrystalline NiO and CoO", Acta. Met., 25, 1307 (1977).

20. P. A. Urick and M. R. Notis, "Final Stage Densification During Pressure-Sintering of CoO", J. Amer. Ceram. Soc., 56 [11] 570 (1973).

21. W. D. Kingery, H. K. Brown, and D. R. Uhlmann, p. 777 Introduction to Ceramics, 2nd Edition, J. Wiley and Sons, (1976).

22. D. R. Petrak, D. T. Rankin, R. Ruh, and R. D. Sisson, "Effect of Porosity on the Elastic Moduli of CoO, CoO-MgO Solid Solutions and $CoAl_2O_4$", J. Amer. Ceram. Soc., 58 [1-2] 78 (1975).

23. ETEC Corporation, Application Note for Vistascan (Video Information Storage and Processing System).

24. M. I. Mendelson, "Average Grain Size in Polycrystalline Ceramics", J. Amer. Ceram. Soc., 52 [8] 443 (1969).

25. J. C. Wurst and J. A. Nelson, "Lineal Intercept Technique for Measuring Grain Size in Two-Phase Polycrystalline Ceramics", J. Amer. Ceram. Soc., 55 [2] 109 (1972).

26. S. A. Saltikov, "The Determination of the Size Distribution of Particles in an Opaque Material from a Measurement of the Size Distribution of their Sections", p. 163 Stereology,

ed. Hans Elias, Springer-Verlag, New York (1967).

27. B. Francois and W. D. Kingery, " The Sintering of Crystalline Oxides, II. Densification and Microstructure Development in UO_2", p. 499 Sintering and Related Phenomena, ed. Kuczynski et al., Gordon and Breach, New York (1967).

28. A. A. Solomon, "Effects of Entrapped Gases in ZnO, I. Sintering and Microstructure Evolution", to be published in J. Amer. Ceram. Soc.

29. C. S. Smith, "Grains, Phases, and Interfaces: An Interpretation of Microstructure, Trans. AIME, 175, 15 (1948).

30. J. E. Burke and J. H. Rosolowski, "Sintering", p. 621 Treatise on Solid State Chemistry Vol. 4, ed. N. B. Hannay, Plenum Press, New York (1970).

31. Discussion (p. 442-444) at end of paper by R. L. Coble and T. K. Gupta, "Intermediate Stage Sintering", p. 423 Sintering and Related Phenomena, ed. Kuczynski et al., Gordon and Breach, New York (1967).

32. O. J. Whittemore, Jr., "Pore Morphology in Ceramic Processing", p. 125 Processing of Crystalline Ceramic, Mat. Sci. Reas. Vol. 11, ed. R. F. Davis, H. Palmour III, T. M. Hare, Plenum Press, New York (1978).

33. D. Uskokovic, U. Petrovic, M. M. Ristic, "Interdependence of the Porosity, Grain Size and Pore Size Changes During Intermediate Stage of Sintering", Presented at the Fifth

International Conference on Sintering and Related Phenomena, July 18-20, 1979, Notre Dame, Indiana.

34. E. H. Aigeltinger and J. P. Drolet, "Modern Developments in Powder Metallurgy", Vol. 6, p. 323, H. H. Hausner and W. E. Smith, ed., Metal Powder Ind. Federation, New York (1979).

APPENDIX 1

Mercury Porosimetry

In order to check the accuracy of our porosity measurements, certain samples were sent out to an independent laboratory (Micromeritics Instrument Corporation) and were analyzed on a Mercury Intrusion Porosimeter. Mercury intrusion is a useful method for characterizing pore size distributions of ceramics.

The method was first proposed by Washburn in 1921, but not until 1945 did Ritter and Drake report applications.[32] Washburn gave the relation for intrusion of a pore of circular opening as $pd = -4 \sigma \cos \theta$, where p is the pressure required to force liquid into a pore of entry diametered, σ is the liquid surface tension and θ is the liquid solid contact angle.

In the mercury intrusion method,[32] a non-wetting liquid is required (θ must be larger than 90°) and mercury is most convenient. The surface tension can be considered constant, and wetting angles are found to range from 130° to 140°C for most materials. Therefore, only the pressure of intrusion needs to be measured to determine the pore diameter. When the volumes of intruded mercury are determined at increasing pressures, a plot of the pore size distribution can be constructed. Pores ranging from 200 μm down to 3 nm can be measured. Additional information can be obtained by constructing pore volume frequency plots.

The values obtained for the net pore volume by mercury porosimetry and our porosity measurements are listed below.

	Mercury Porosimetry	Present Investigation
SAMPLE A	.041 cc/g	.039 cc/g
SAMPLE B	.033 cc/g	.035 cc/g

These results confirm the accuracy of our methods.

APPENDIX 2

Saltikov Method for Determination of Size Distribution of Particles[26]

The Saltikov method is used for determining particle size distribution based on the principle that the distribution of random cross-sectional areas of any body depends only on its shape. The method is applicable to both spherical and non-spherical particles.

The first step in this method is to obtain the size of the pore with the maximum diameter in the field being examined. Once the maximum diameter (D_M) is known it is multiplied by the constant values given in Table 1A to obtain the class interval diameter (D_k) to be studied.

TABLE 1A
Class Interval Constants (K)

1) 1.000	5) 0.3981	9) 0.1581
2) 0.7943	6) 0.3162	10) 0.1259
3) 0.6310	7) 0.2512	11) 0.1000
4) 0.5012	8) 0.1995	12) 0.0794, etc.

Measurements of the total number of particles per unit area less than D_k (N_{Ak}) are now taken for each of the class interval

diameters calculated. In fact, the Oversize Count procedure on the Millipore πMC is such that the values must be taken going first from the smallest class interval diameter to the largest rather than vice versa. Once values for N_{Ak} are known, the number of particles per unit volume in the k_{th} class interval is calculated from the following formula:

$$N_{Vk} = \frac{1}{D_k} [1.6461\ N_{Ak} - 0.4561\ N_{A(k-1)} - 0.1162\ N_{A(k-2)} - 0.0415\ N_{A(k-3)} - 0.0173\ N_{A(k-4)} - 0.0079\ N_{A(k-5)} - 0.0038\ N_{A(k-6)} - 0.0018\ N_{A(k-7)} - 0.0010\ N_{A(k-8)} - 0.0003\ N_{A(k-9)} - 0.0002\ N_{A(k-10)} - 0.0002\ N_{A(k-11)}]$$

where for D_k we substitute D_1, D_2, D_3, etc. depending on the class interval of concern.

In using the above equation, the calculation for a given class interval of pores is continued only until the index N_{Ak} reduces to zero. For example, for the fifth class interval (N_{V5}) the first five terms in the brackets are used. Only for the 12th class interval (N_{V12}) are all the terms used. Therefore, from the above equation, a plot of N_V vs. d can be obtained.

VITA

Andrew David Miro was born on August 12, 1955, at Doctor's Hospital in New York City, New York to Dr. and Mrs. Raymond I. Miro.

Mr. Miro was graduated from Herricks Senior High School in New Hyde Park, New York in June 1973. He then attended the State University of New York, College of Ceramics at Alfred University. He graduated from Alfred in June 1977, receiving the B.S. degree in Ceramic Science and the B.A. degree in Chemistry. He started the M.S. program at Lehigh University in August, 1977.